Probing the Role of Metal Ions in RNA Catalysis: Kinetic and Thermodynamic Characterization of a Metal Ion Interaction with the 2′-Moiety of the Guanosine Nucleophile in the *Tetrahymena* Group I Ribozyme[†]

Shu-ou Shan and Daniel Herschlag*

Department of Biochemistry, Stanford University, Stanford, California 94305-5307

Received February 17, 1999; Revised Manuscript Received May 14, 1999

ABSTRACT: Deciphering the role of individual metal ions in RNA catalysis is a tremendous challenge, as numerous metal ions coat the charged backbone of a folded RNA. Metal ion specificity switch experiments combined with quantitative analysis may provide a powerful tool for probing specific metal ion–RNA interactions and for delineating the role of individual metal ions among the sea of metal ions bound to RNA. We show herein that Mn^{2+} rescues the deleterious effect of replacing the 2′-OH of the guanosine nucleophile (G) by $-NH_2$ (G_{NH_2}) in the reaction catalyzed by the *Tetrahymena* group I ribozyme (E), and the Mn^{2+} concentration dependence suggests that a single metal ion is responsible for rescue. This provides strong evidence for a metal ion interaction with the 2′-moiety of G in this ribozyme (referred to as M_C), confirming and extending previous results in a bacteriophage group I intron [Sjögren, A.-S., Pettersson, E., Sjöberg, B.-M., and Strömberg, R. (1997) *Nucleic Acids Res. 25*, 648–654]. Toward understanding the $>10^6$-fold catalytic contribution of the 2′-OH of G, we have determined the individual reaction steps affected by M_C and quantitated these effects. Mn_C^{2+} has only a small effect on binding of G_{NH_2} to the free ribozyme or ribozyme·oligonucleotide complexes that lack the reactive phosphoryl group. In contrast, Mn_C^{2+} increases the binding of G_{NH_2} to the ribozyme·oligonucleotide substrate (E·S) complex 20-fold and increases the binding of S to the $E·G_{NH_2}$ complex by the same amount. These and other observations suggest that M_C plays an integral role in the coupled binding of the oligonucleotide substrate and the guanosine nucleophile. This metal ion may be used to align the nucleophile within the active site, thereby facilitating the reaction. Alternatively or in addition, M_C may act in concert with an additional metal ion to coordinate and activate the 3′-OH of G. Finally, these experiments have also allowed us to probe the properties of this metal ion site and isolate the energetic effects of the interaction of this specific metal ion with the 2′-moiety of G.

Divalent metal ions are essential for the structure and function of RNA. Numerous metal ions typically coat an RNA to neutralize the backbone charges and stabilize tertiary contacts, facilitating the folding of RNA into specific three-dimensional structures (e.g., *2–19* and references cited therein). In addition to these structural roles, specific active site metal ions also directly participate in the chemical transformations catalyzed by many RNA enzymes (e.g., *20–26*). However, the sea of metal ions bound to RNA presents an enormous challenge to deciphering the role of individual metal ions in RNA catalysis.

Specific metal ion ligands have been identified by metal ion specificity switch experiments (*20–32*). These experiments exploit the preference of nitrogen and sulfur ligands to interact more strongly with soft metal ions, such as Mn^{2+}, than with hard metal ions, such as Mg^{2+}. The identification of metal ion ligands provides a starting point for deciphering the role of metal ions in RNA catalysis, yet a number of questions remain unanswered: How many metal ions are

there at an RNA active site? Which ribozyme groups provide additional ligands for each metal ion? How much does each metal ion contribute to catalysis? Which reaction step(s) do-(es) each metal ion affect? And finally, how does each metal ion exert its catalytic role?

We have combined the approach of metal ion specificity switch with quantitative kinetic and thermodynamic analysis to address these questions with the well-characterized *Tetrahymena* ribozyme (E).[1] This ribozyme, derived from the self-splicing *Tetrahymena* group I intron, catalyzes a transesterification reaction in which an exogenous guanosine

---

[1] Abbreviations: E is the *Tetrahymena* ribozyme; S refers to the oligonucleotide substrate $CCCUCUA_5$ or $CCUCUA_5$, without specification of the sugar identity; P refers to the oligonucleotide product $CCCUCU_{OH}$ or $CCUCU_{OH}$, without specification of the sugar identity; P1 is the duplex formed between the internal guide sequence (IGS) of the ribozyme and the oligonucleotide substrate or product; G_{NH_2} and $G_{NH_3^+}$ refer to deprotonated and protonated 2′-aminoguanosine, respectively; G_N refers to G_{NH_2} or $G_{NH_3^+}$, without specification of the protonation state of the 2′-amino group; and G_X refers to G or G_N. The parentheses in E(·S), E(·G), and other complexes denote that ribozyme forms both with and without the bound substrates are described; e.g., E(·S) refers to both E and the E·S complex. The individual oligonucleotide substrates and products used in this study are defined in Chart 1.
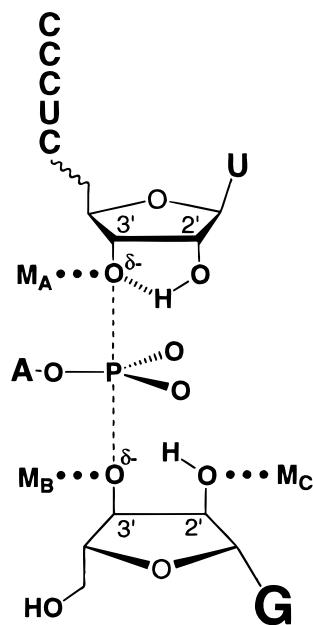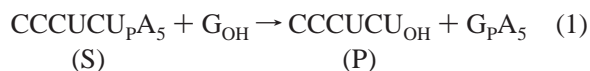
FIGURE 1: Metal ion interactions in the transition state of the *Tetrahymena* ribozyme reaction. The dashed lines (---) depict the partial bonds between the reactive phosphorus and the 3′-oxygen of S and the 3′-oxygen of G, and 'δ-' depicts the partial negative charges on the 3′-oxygens of S and G. M_A is the metal ion that interacts with the 3′-oxygen of U(−1) of S identified by Piccirilli et al. (*20*), M_B is the metal ion interacting with the 3′-moiety of G identified by Weinstein et al. (*25*), and M_C is the metal ion interacting with the 2′-moiety of G identified by Sjögren et al. in a bacteriophage T4 group 1 intron (*22*) and extended to the *Tetrahymena* ribozyme in this work. Recent results suggest that M_A, M_B, and M_C are three distinct metal ions (Shan et al., submitted).

nucleophile (G) cleaves a specific phosphodiester bond of an oligonucleotide substrate (S) that mimics the 5′-splice site (eq 1; *33−35*).

$$\text{CCCUCU}_\text{P}\text{A}_5 + \text{G}_\text{OH} \rightarrow \text{CCCUCU}_\text{OH} + \text{G}_\text{P}\text{A}_5 \quad (1)$$
$$\text{(S)} \qquad\qquad\qquad \text{(P)}$$

Metal ion specificity switch experiments have identified metal ion interactions with the 3′-leaving group oxygen of S and with the 3′-OH of G in the *Tetrahymena* ribozyme reaction [Figure 1, M_A and M_B, respectively (*20, 25*)], and a metal ion interaction with the 2′-OH of G has been identified in a self-splicing group I intron from bacteriophage T4 (*22*). In this work, the metal ion interaction with this 2′-OH group has been extended to the *Tetrahymena* ribozyme (Figure 1, M_C). Further, investigation of the well-characterized *Tetrahymena* ribozyme allowed dissection of the effect of M_C on individual reaction steps. This has further allowed the affinities of M_C for the ribozyme and ribozyme·substrate complexes to be determined, the effects of M_C to be distinguished from those of other metal ions, and the energetics of the interactions of M_C with the 2′-moiety of G to be quantitated.

MATERIALS AND METHODS

Materials. Ribozyme was prepared by in vitro transcription with T7 RNA polymerase as described previously (*36*). Oligonucleotides were made by solid phase synthesis and supplied by the Protein and Nucleic Acid Facility at Stanford

Chart 1[a]

abbreviation	oligonucleotide substrate or product										
		-5		-3		-1	+1	+2		+4	
rSA$_5$	rC	rC	rC	rU	rC	rU	rA	rA	rA	rA	rA
-1d,rSA$_5$	rC	rC	rC	rU	rC	dT	rA	rA	rA	rA	rA
-1d,rSA$_5$'		rC	rC	rU	rC	dT	rA	rA	rA	rA	rA
dSA$_5$	dC	dC	dC	dU	dC	dT	dA	dA	dA	dA	dA
-1f$_2$,dSA$_5$	dC	dC	dC	dU	dC	f$_2$T	dA	dA	dA	dA	dA
rP	rC	rC	rC	rU	rC	rU					
rP'		rC	rC	rU	rC	rU					
rS$_{Me}$	rC	rC	rC	rU	rC	rU$_{Me}$					

[a] r = 2′-OH; d = 2′-H; f$_2$ = 2′,2′-F$_2$; Me = P(O$_2$)-OCH$_3$.

University or were gifts from L. Beigelman (Ribozyme Pharmaceuticals Inc.). Oligonucleotide substrates (Chart 1) were 5′-end-labeled using [γ-^{32}P]ATP and T4 polynucleotide kinase and purified by electrophoresis on 24% nondenaturing polyacrylamide gels, as described previously (*36, 37*). Oligonucleotides for inhibition studies were purified by ion-exchange HPLC. 2′-Aminoguanosine (G_N) was a gift from F. Eckstein.

General Kinetic Methods. All reactions were single-turnover, with ribozyme in excess of labeled oligonucleotide substrate (S*). Reactions were carried out at 30 °C in 50 mM buffer (NaEPPS or NaHEPES), with a background of 10 mM MgCl$_2$ and varying concentrations of MnCl$_2$ or ZnCl$_2$ unless otherwise specified. Each rate and equilibrium constant was determined at a series of Mn^{2+} concentrations, and, in some cases, the Mg^{2+} concentration was also varied.

Reactions were followed and analyzed essentially as previously described (*33, 38*). Briefly, ribozymes were preincubated for 30 min in 10 mM MgCl$_2$ and 50 mM buffer at 50 °C and cooled to 30 °C, and Mg^{2+}, Mn^{2+}, and Zn^{2+} were added to obtain the desired metal ion concentrations prior to initiating the reaction by addition of S* (<0.1 nM). Six 2 μL aliquots of the reaction mixture were removed from 20 μL reactions at specified times, and further reaction was quenched by addition of 4 μL of stop solution [90% formamide with EDTA in ≥2-fold excess of total divalent metal ion (20−200 mM), 0.005% xylene cyanole, 0.01% bromophenol blue, and 1 mM Tris, pH 7.5]. Oligonucleotide substrates and products were separated by electrophoresis on 20% polyacrylamide/7 M urea gels, and their ratio at each time point was quantitated with a Molecular Dynamics Phosphorimager.

Reactions were followed for ≥$3t_{1/2}$ except for very slow reactions. Good first-order fits to the data, with end points of ≥90%, were obtained (KaleidaGraph, Synergy Software, Reading, PA). The slow reactions were typically linear for up to 20 h, and an end point of 95% was assumed to obtain observed rate constants from the initial rates.

Following the Binding and Reactivity of Neutral G_{NH_2}. Analysis of the metal ion interaction with deprotonated 2′-aminoguanosine (G_{NH_2}) could be obscured by protonated 2′-aminoguanosine ($G_{NH_3^+}$), which is a strong inhibitor of the ribozyme reaction and weakens the binding of M_C (*39*). Comparison of the pH dependences of the reaction of 2′-aminoguanosine (G_N) relative to that of G indicated that the

binding and reactivity of G_{NH_2} in 10 mM Mg^{2+} can be followed above pH 7.9 [Under these conditions (10 mM Mg^{2+}, 30 °C), $G_{NH_3^+}$ deprotonates with a pK_a of 6.1 in aqueous solution and with pK_a values of $\sim$7.0 and 7.5 in the $E \cdot G_N$ and $E \cdot S \cdot G_N$ complexes, respectively (*39*)]. Varying the pH from 7.9 to 8.5 does not significantly change the binding of G_N, the binding of S to $E \cdot G_N$, or the rate of reaction of G_N relative to G, suggesting that the 2'-amino group is predominantly deprotonated. With Mn_C^{2+} bound, the pK_a of the 2'-amino group is below 5 in the $E \cdot S \cdot G_N$ complex (*39*); this allows the dissociation constant of S from the $E \cdot S \cdot G_{NH_2}$ complex to be determined at lower pH.

Kinetic Constants. The nomenclature used for rate constants is defined in Chart 2. $k_c^{G_X}$, a first-order rate constant,

Chart 2

rate constant	reaction
$k_c^{G_X}$	$E \cdot S \cdot G_X \rightarrow$ products
$(k_c/K_m)^{G_X}$	$E \cdot S + G_X \rightarrow$ products
$(k_c/K_m)^S$	$E \cdot G_X + S \rightarrow$ products
$k_3^{G_X}$	$E + S + G_X \rightarrow$ products

was measured for the oligonucleotide substrate -1d,rSA$_5$ (Chart 1), and was determined with ribozyme saturating with respect to S (200 nM E, $K_d^S < 0.5$ nM; unpublished results) and with saturating G_X (2 mM). The second-order rate constant $(k_c/K_m)^{G_X}$ was also determined for -1d,rSA$_5$ with E saturating with respect to S as above, but with G_X subsaturating (at least three G_X concentrations, each >5-fold below the dissociation constant). The second-order rate constant $(k_c/K_m)^S$ was determined for the oligonucleotide substrate rSA$_5$ (Chart 1) with saturating G_X (2 mM) but with E subsaturating with respect to S (0.2−1 nM E, $K_m^S >$ 10 nM; unpublished results). $k_3^{G_X}$, the third-order rate constant, was determined for the oligonucleotide substrate dSA$_5$ (Chart 1) with both E and G_X subsaturating [10−30 nM E, $K_d^S \approx$ 150 nM (unpublished results); G_X concentrations were at least 5-fold below their dissociation constants].

Determination of the Dissociation Constant of G and G_{NH_2}. (A) Binding of G and G_{NH_2} to E·S. Dissociation constants of G and G_{NH_2} from the $E \cdot S \cdot G_X$ ternary complex, $K_d^{G_{X}'}$, were determined with -1d,rSA$_5$ (Chart 1) with ribozyme saturating with respect to S (50-200 nM E, $K_d^S \leq 0.5$ nM). $K_d^{G_{X}'}$ values were obtained by following the reaction rate with varying concentrations of G_X (1−2000 μM). Under the conditions of these reactions, the concentration of G_X that provides half of the maximal rate, $K_{1/2}^{G_X}$, equals $K_d^{G_{X}'}$, as described previously (*38*). The data were fit to eq 2, in which k_{obsd} is the observed rate constant at a particular G_X concentration and k_{max} is the rate constant with saturating G_X.

$$k_{obsd} = k_{max} \times \frac{[G_X]}{[G_X] + K_{1/2}^{G_X}} \quad (2)$$

(B) Binding of G and G_{NH_2} to Free E. Dissociation constants of G_X from the $E \cdot G_X$ binary complex, $K_d^{G_X}$, were determined analogously under conditions such that S is not bound at the ribozyme active site. This was accomplished by using the oligonucleotide substrate dSA$_5$ (Chart 1), which binds E more weakly than -1d,rSA$_5$ (*40*), and by using ribozyme subsaturating with respect to dSA$_5$ [10-30 nM E,

$K_d^S \sim$ 150 nM; unpublished results)]. As a control, binding of G_X to E was also measured with another weak-binding oligonucleotide substrate, -1f$_2$,dSA$_5$ (Chart 1; *40* and D.H., unpublished results), and the values of $K_d^{G_X}$ obtained were the same, within experimental error (30%; data not shown).

(C) Binding of G_{NH_2} to E·P. Binding of G_{NH_2} to the ribozyme·oligonucleotide product (E·P) complex was determined by two independent methods, which yielded the same dissociation constant of G_{NH_2} within experimental error (20%). (1) The rate of miscleavage of P (CCCUCU) was followed with varying concentrations of G_{NH_2} and fit to eq 2. In the normal reaction, the P1 duplex, formed between the oligonucleotide and the ribozyme's internal guide sequence (IGS), docks into tertiary interactions with the ribozyme core to align the phosphodiester of the normal cleavage site, which is specified by the conserved G·U wobble pair. Miscleavage can occur when the P1 duplex transiently docks into tertiary interactions with an alternative phosphodiester aligned at the cleavage site (*41, 42*). This miscleavage reaction can be used to probe properties of the ground-state E·P complex, as described previously (*43*). Miscleavage reactions were carried out with trace amounts of labeled oligonucleotide product ([P*] < 0.1 nM) with E saturating with respect to P (50-200 nM E, $K_d^P \leq 0.1$ nM; unpublished results) as described previously (*43*). The following observations suggest that the chemical step is rate-determining for miscleavage and that equilibrium binding of G_{NH_2} to the E·P complex is established prior to the cleavage step: (i) the maximal rate observed with saturating G_{NH_2} is slow ($k_{max} < 10^{-4}$ min^{-1}); (ii) the value of k_{max} has a log-linear dependence on pH (*43* and data not shown); (iii) no lag phase was observed in reaction time courses. Thus, the $K_{1/2}^{G_{NH_2}}$ obtained reflects the equilibrium dissociation constant of G_{NH_2} from $E \cdot P \cdot G_{NH_2}$. (2) G_{NH_2} was used as a competitive inhibitor of the reverse reaction (eq 3a), as G_{NH_2} can bind to E·P, thereby preventing binding and reaction of 5'-labeled G_PA (*G_PA). With E·P subsaturating with respect to *G_PA [<0.1 nM; 0.2−1 μM E·P; $K_d^{G_PA} \geq 300$ μM (*44* and R. Russell and D.H., unpublished results)], the inhibition constant, K_i, equals the dissociation constant of G_{NH_2} from $E \cdot P \cdot G_{NH_2}$. Values of K_i were obtained from the dependence of the observed rate constant of the reverse reaction (k_{obsd}) on the concentration of inhibiting G_{NH_2} according to eq 3b, which was derived from eq 3a.

$$E \cdot CCCUCU_{OH} + {}^*G_PA \xrightarrow{k_o} E \cdot CCCUCU_PA + {}^*G_{OH} \quad (3a)$$
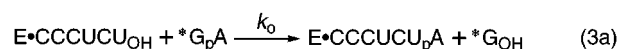
$$K_i \parallel \pm G_{NH_2}$$

$$E \cdot CCCUCU_{OH} \cdot G_{NH_2}$$

$$k_{obsd} = k_o \times \frac{K_i}{K_i + [G_{NH_2}]} \quad (3b)$$

Determination of the Equilibrium Constants for Binding of Oligonucleotide Substrates and Products. The equilibrium constant for binding of S was determined with the shortened oligonucleotide substrate CCUCdTA$_5$, because initial experiments indicated that binding equilibrium could not be obtained prior to cleavage of the full-length substrate CCCUCdTA$_5$. This substrate binds the ribozyme very tightly,

such that the chemical step is faster than its dissociation at the high pH and Mn^{2+} concentrations necessary to follow reactions of G_{NH_2} (unpublished results). Removing a nucleotide at the 5′-terminus of S weakens the stability of the P1 duplex formed between the oligonucleotide substrate and the internal guide sequence of E (see preceding section), but has no significant effect on tertiary interactions between the P1 duplex and the ribozyme core, binding of G and G_{NH_2}, or the chemical step (*45* and references cited therein; Narlikar et al., submitted; unpublished results). This allows the binding of S to be directly measured from concentration dependences in kinetic experiments.

(A) Binding of S to Free E. The dissociation constant of S ($CCUCdTA_5$) from the E·S binary complex, K_d^S, was measured with subsaturating G ($\leq 10\ \mu M$) and was determined using two independent methods, which yielded the same value of K_d^S within experimental error (40%). (1) The observed rate constant of reaction (k_{obsd}) was followed at varying concentrations of E (0.2-50 nM) under conditions that ensure that the chemical step is slower than dissociation of S (pH < 7.0; k_{obsd} < 0.01 min^{-1} vs $k_{off}^S \geq 0.025$ min^{-1}). Thus, K_d^S is equal to $K_{1/2}^S$, the concentration of E that provides the half-maximal rate, and was obtained from a nonlinear least-squares fit of the concentration dependence to eq 4, in which k_{max} is the rate constant with saturating E.

$$k_{obsd} = k_{max} \times \frac{[E]}{[E] + K_{1/2}^S} \tag{4}$$

(2) The dissociation constant of S was also obtained from the rate constants for binding and dissociation of S, k_{on}^S and k_{off}^S, respectively, according to the relationship $K_d^S = k_{off}^S/k_{on}^S$. The value of k_{off}^S was determined by pulse−chase measurements as described previously (*33, 37, 38, 46*). The k_{on}^S value for $CCUCdTA_5$ was assumed to be the same as that for rSA_5, as removal of the 5′ C residue or substitution of the 2′-OH of U(−1) with 2′-H has no effect on k_{on}^S in the presence of 10 mM Mg^{2+} (*40* and Narlikar et al., submitted). The values of k_{on}^S for rSA_5 in the presence of Mn^{2+} were determined by measuring $(k_c/K_m)^{S,app}$, the apparent second-order rate constant for the reaction: E + S* → products. The observed $(k_c/K_m)^{S,app}$ value for rSA_5 is equal to k_{on}^S at subsaturating concentrations of G, because essentially each molecule of S* that binds E is cleaved rather than dissociates from E·S* (*33, 47*).

The dissociation constants of S from the E·S·G_X ternary complexes, $K_d^{S'}$, were measured using equilibrium binding and pulse−chase experiments analogous to those described above, except that saturating concentrations of G_X (2 mM) were used. Below 2 mM Mn^{2+}, the dissociation constant of S from the E·S·G_{NH_2} complex was measured at pH 7.9−8.5 to prevent partial protonation of G_{NH_2} (*39*; see also above). At 5 mM Mn^{2+}, however, dissociation of S is slower than the chemical step of G_{NH_2} above pH 7.9 even with the shortened substrate. Because the pK_a of the 2′-amino group in the E·S·G_N complex is lowered to ≤ 5 at this Mn^{2+} concentration (*39*), the pH could be lowered to 7.2; this slows the chemical step, allowing equilibrium binding prior to cleavage and measurement of the dissociation constant of S from E·S·G_{NH_2}.

(B) Binding of P to E·G_{NH_2}. The dissociation constant of the oligonucleotide product from the E·P·G_{NH_2} complex (K_d^P) was determined using P as a competitive inhibitor of the reaction of rSA_5 (S*; eq 5a). Under conditions such that

$$E \cdot G_{NH_2} + S^* \xrightarrow{k_o} \text{products} \tag{5a}$$

$$K_i \updownarrow \pm P$$

$$E \cdot P \cdot G_{NH_2}$$

$$k_{obsd} = k_o \times \frac{K_i}{K_i + [P]} \tag{5b}$$

E (0.2−1 nM) is subsaturating with respect to S* and G_{NH_2} is saturating (2 mM), the inhibition constant K_i is equal to K_d^P. However, initial experiments indicated that the full-length oligonucleotide product CCCUCU binds E tightly, with a dissociation constant of ≤ 0.1 nM (unpublished results). Thus, addition of CCCUCU results in titration of E·G_{NH_2} even with E concentrations of ~ 0.1 nM, so that an equilibrium binding constant could not be obtained (*48*). To avoid this titration behavior, a shortened oligonucleotide product, CCUCU, was used. Removing the 5′ C of P weakens the stability of the P1 duplex but has no effect on other reaction steps, as described in the preceding section for the case with the shortened oligonucleotide substrate. The dependence of the observed rate constant of reaction of S* (k_{obsd}) on the concentration of P was fit to eq 5b, which was derived from eq 5a. In these experiments, P was preincubated with E for >5 min prior to addition of S*. Varying the time of preincubation did not affect the observed rate constants, and the reactions followed good first-order kinetics, suggesting that equilibrium binding between P and E was established prior to initiation of the reactions.

Determination of the Affinity of Mn_C^{2+} for the Ribozyme and Ribozyme·Substrate Complexes. As described under Results, Mn^{2+} alters the equilibrium constants for binding of G_{NH_2}, the affinity of S for E·G_{NH_2} relative to that for E(·G), and the rate of reaction of G_{NH_2} relative to G. The Mn^{2+} concentration dependences of these changes are consistent, in all cases, with the effect expected for a single Mn^{2+} (referred to as Mn_C^{2+} throughout). The following strongly suggest that $K_{1/2}^{Mn}$, the concentration of Mn^{2+} required to reach half-saturation, equals $K^{Mn,app}$, the equilibrium dissociation constant of Mn_C^{2+}: (i) the rate of reaction is not affected by the time of incubation with Mn^{2+} before initiation of the reaction or by the order of addition of Mn^{2+} and other reaction components; (ii) reactions follow good first-order kinetics without a lag phase; (iii) the $K_{1/2}^{Mn}$ value is not affected by alternative substrates or by changing pH, changes that alter the observed rate of reaction. These observations suggest that Mn^{2+} achieves equilibrium binding prior to the chemical step, consistent with previous results that suggest that the exchange of bound metal ions is fast relative to the chemical step (*47*). The superscript 'app' accompanying the K^{Mn} values denotes that these are apparent dissociation constants of Mn_C^{2+} at a particular Mg^{2+} concentration, because Mn_C^{2+} competes with a Mg^{2+} bound at metal site C under the experimental conditions, as described under Results.

In eqs 6, 8, and 10 below, the Mn^{2+} concentration dependences of the relative rate and equilibrium constants for G_{NH_2} were used to obtain the affinity of Mn_C^{2+}. In all cases, the Mn^{2+} effects specific to G_{NH_2} are observed well below 1 mM Mn^{2+}, whereas the effects of Mn^{2+} at higher concentrations are similar for reactions of both G and G_{NH_2}. The use of relative rate and equilibrium constants provides controls for these nonspecific Mn^{2+} effects. Further, the Mn^{2+} concentration dependence of the rate of reaction with G is the same at lower pH values (5.6–7.1; data not shown), suggesting that the plateau of the reaction rates at high Mn^{2+} concentrations (above 10 mM) does not arise from precipitation of Mn^{2+} at high pH.

The use of relative rate and equilibrium constants in the analyses of eqs 6, 8, and 10 assumes that replacing Mg_C^{2+} with Mn_C^{2+} has no effect on the reaction of G and that any additional Mn^{2+} ions that affect the G reaction have the same effect on the G_{NH_2} reaction. The following observations strongly support these assumptions (see also Results): (i) the data are fit well by eqs 6, 8, and 10, which were derived with these assumptions; (ii) over the range of Mn^{2+} concentrations that rescue[2] the G_{NH_2} reaction, there is no significant change in the rate and equilibrium constants of the reaction of G; (iii) the Mn^{2+} effect on the G reaction that occurs at higher Mn^{2+} concentrations is eliminated by modification of the A(+1) residue of S without affecting rescue of the reaction of G_{NH_2} by Mn^{2+} (unpublished results).

(A) Binding of Mn_C^{2+} to E·S, $K_{E·S}^{Mn,app}$. Mn^{2+} increases the reactivity of G_{NH_2} relative to G in the reaction: $E·S + G_X \rightarrow$ products $[(k_c/K_m)^{G_X}]$, providing a signal for the binding of Mn_C^{2+} to E·S. The apparent dissociation constant of Mn_C^{2+} from the E·S complex, $K_{E·S}^{Mn,app}$, was obtained by nonlinear least-squares fit of the Mn^{2+} concentration dependence of $(k_c/K_m)^{rel}$ [= $(k_c/K_m)^{G_{NH_2}}/(k_c/K_m)^G$] to eq 6, which was derived from Scheme 2 in the Results. $(k_c/K_m)_{obsd}^{rel}$ is the observed rate constant for reaction of G_{NH_2} relative to G at a particular Mn^{2+} concentration, and $(k_c/K_m)_{Mg}^{rel}$ and $(k_c/K_m)_{Mn}^{rel}$ are the relative reactivities of G_{NH_2} with zero and saturating Mn^{2+}, respectively.

$$(k_c/K_m)_{obsd}^{rel} = (k_c/K_m)_{Mg}^{rel} \times \frac{K_{E·S}^{Mn,app}}{K_{E·S}^{Mn,app} + [Mn^{2+}]} +$$
$$(k_c/K_m)_{Mn}^{rel} \times \frac{[Mn^{2+}]}{K_{E·S}^{Mn,app} + [Mn^{2+}]} \quad (6)$$

The affinity of Mn_C^{2+} for E·S was also determined from the increase in the binding of G_{NH_2} to E·S ($K_b^{G_{NH_2}\prime}$) with added Mn^{2+} (see Results). As the binding of G is the same in the presence and absence of Mn^{2+}, there is no need to correct for the effect of Mn^{2+} on G binding. The Mn^{2+} concentration dependence of $K_b^{G_{NH_2}\prime}$ was therefore fit to eq 7, which was derived from Scheme 4 in the Results. $K_{b,obsd}^{G_{NH_2}\prime}$ is the observed binding constant of G_{NH_2} at a particular Mn^{2+} concentration, and $K_{b,Mg}^{G_{NH_2}\prime}$ and $K_{b,Mn}^{G_{NH_2}\prime}$ are the binding constants of G_{NH_2} with zero and saturating Mn^{2+}, respectively.

$$K_{b,obsd}^{G_{NH_2}\prime} = K_{b,Mg}^{G_{NH_2}\prime} \times \frac{K_{E·S}^{Mn,app}}{[Mn^{2+}] + K_{E·S}^{Mn,app}} +$$
$$K_{b,Mn}^{G_{NH_2}\prime} \times \frac{[Mn^{2+}]}{[Mn^{2+}] + K_{E·S}^{Mn,app}} \quad (7)$$

(B) Binding of Mn_C^{2+} to E, $K_E^{Mn,app}$. Mn^{2+} increases the reactivity of G_{NH_2} relative to G in the reaction $E + S + G_X \rightarrow$ products ($k_3^{G_X}$), providing a signal for the binding of Mn_C^{2+} to free E. The apparent dissociation constant of Mn_C^{2+} from E, $K_E^{Mn,app}$, was obtained from nonlinear least-squares fit of the Mn^{2+} concentration dependence of k_3^{rel} (= $k_3^{G_{NH_2}}/k_3^G$) to eq 8, which was derived from Scheme 5 in the Results. $k_{3,obsd}^{rel}$ is the observed relative reactivity of G_{NH_2} at a particular Mn^{2+} concentration, and $k_{3,Mg}^{rel}$ and $k_{3,Mn}^{rel}$ are the relative reactivities of G_{NH_2} with zero and saturating Mn^{2+}, respectively.

$$k_{3,obsd}^{rel} = k_{3,Mg}^{rel} \times \frac{K_E^{Mn,app}}{[Mn^{2+}] + K_E^{Mn,app}} +$$
$$k_{3,Mn}^{rel} \times \frac{[Mn^{2+}]}{[Mn^{2+}] + K_E^{Mn,app}} \quad (8)$$

(C) Binding of Mn_C^{2+} to E·P, $K_{E·P}^{Mn,app}$. The affinity of Mn_C^{2+} for E·P was probed by the Mn^{2+} stimulation of the rate of product miscleavage: $E·P + G_{NH_2} \rightarrow P''$ ($k_{mscl}^{G_{NH_2}}$, see above). The apparent dissociation constant of Mn_C^{2+} from E·P, $K_{E·P}^{Mn,app}$, was determined from the Mn^{2+} concentration dependence of $k_{mscl}^{G_{NH_2}}$. As Mn^{2+} does not affect the rate of miscleavage by G, no Mn^{2+} effect on the reaction: $E·P + G \rightarrow P''$ needs to be corrected. Equation 9 was used, in which $k_{mscl,obsd}^{G_{NH_2}}$ is the rate of miscleavage by G_{NH_2} at a particular Mn^{2+} concentration, and $k_{mscl,Mg}^{G_{NH_2}}$ and $k_{mscl,Mn}^{G_{NH_2}}$ are the rates of miscleavage by G_{NH_2} with zero and saturating Mn^{2+}, respectively.

$$k_{mscl,obsd}^{G_{NH_2}} = k_{mscl,Mg}^{G_{NH_2}} \times \frac{K_{E·P}^{Mn,app}}{[Mn^{2+}] + K_{E·P}^{Mn,app}} + k_{mscl,Mn}^{G_{NH_2}} \times$$
$$\frac{[Mn^{2+}]}{[Mn^{2+}] + K_{E·P}^{Mn,app}} \quad (9)$$

(D) Binding of Mn_C^{2+} to E·S·G_{NH_2}, $K_{E·S·G_{NH_2}}^{Mn,app}$. Addition of Mn^{2+} decreases the dissociation of S from the E·S·G_{NH_2} complex more than it decreases dissociation of S from E·S and E·S·G (see Results). This provides a signal for the binding of Mn_C^{2+} to the E·S·G_{NH_2} complex. Following the analysis described above, the apparent dissociation constant of Mn_C^{2+} from E·S·G_{NH_2}, $K_{E·S·G_{NH_2}}^{Mn,app}$, was obtained from the Mn^{2+} concentration dependence of $K_d^{S,rel}$, the dissociation constant of S from the E·S·G_{NH_2} complex relative to that from the E·S·G complex. Equation 10 was used, which was derived from Scheme 6 in the Results. $K_{d,obsd}^{S,rel}$ is the dissociation constant of S from E·S·G_{NH_2} relative to that from E·S·G at a particular Mn^{2+} concentration, and $K_{d,Mg}^{S,rel}$ and $K_{d,Mn}^{S,rel}$ are the relative dissociation constants of S with zero and saturating Mn^{2+}, respectively.

---

[2] Throughout the text, 'rescue' refers to the increase in the binding and/or the rate of reaction of G_{NH_2} relative to G by added Mn^{2+}.

$$K_{d,obsd}^{S,rel} = K_{d,Mg}^{S,rel} \times \frac{K_{E \cdot S \cdot G_{NH_2}}^{Mn,app}}{[Mn^{2+}] + K_{E \cdot S \cdot G_{NH_2}}^{Mn,app}} +$$

$$K_{d,Mn}^{S,rel} \times \frac{[Mn^{2+}]}{[Mn^{2+}] + K_{E \cdot S \cdot G_{NH_2}}^{Mn,app}} \quad (10)$$

(E) Determination of the Mn^{2+} Specificity of Site C, K^{rel}. The specificity of a metal site for Mn^{2+} relative to Mg^{2+}, K^{rel}, is defined by eq 11:

$$E^{Mg} + Mn \overset{K^{rel}}{\rightleftharpoons} E^{Mn} + Mg \quad (11a)$$
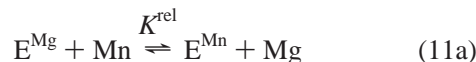
$$K^{rel} = \frac{[E^{Mn}][Mg^{2+}]}{[E^{Mg}][Mn^{2+}]} \quad (11b)$$

in which E^{Mg} and E^{Mn} denote ribozyme forms with the metal site occupied by Mg^{2+} and Mn^{2+}, respectively. The apparent dissociation constant of Mn^{2+} at a particular Mg^{2+} concentration, $K^{Mn,app}$, is defined by eq 12:

$$K^{Mn,app} = \frac{([E_t] - [E^{Mn}]) \times [Mn^{2+}]}{[E^{Mn}]} \quad (12a)$$

$$[E_t] = [E] + [E^{Mn}] + [E^{Mg}] \quad (12b)$$

in which $[E_t]$ denotes the total concentration of all ribozyme forms and E denotes the ribozyme form with the metal site unoccupied. If the metal site is predominantly occupied by either Mg^{2+} or Mn^{2+} (see Results), eq 12a reduces to eq 13:

$$K^{Mn,app} \approx \frac{[E^{Mg}][Mn^{2+}]}{[E^{Mn}]}; \; [E] \ll [E^{Mg}] + [E^{Mn}] \quad (13)$$

Combining eq 13 with eq 11b gives eq 14, which is used to calculate the Mn^{2+} specificity of metal site C in Table 1:

$$K^{rel} \approx [Mg^{2+}]/K^{Mn,app} \quad (14)$$

RESULTS

We first describe results that suggest that a single Mn^{2+} ion rescues the reaction of G_{NH_2} with the *Tetrahymena* ribozyme (Figure 1, M_C), analogous to the metal ion interaction observed previously in a bacteriophage T4 group I intron (22). To understand the role of M_C in catalysis, the effects of the Mn^{2+} ion bound at site C (Mn_C^{2+}) on individual steps of the *Tetrahymena* ribozyme reaction have been isolated. These experiments are described in the second section and are summarized in the thermodynamic and kinetic framework of Scheme 1. This analysis reveals a communication between Mn_C^{2+} and the oligonucleotide substrate (S). The final section explores the group(s) on S responsible for this communication.

A Mn^{2+} Ion Increases the Reactivity of G_{NH_2} Relative to G in the Reaction: $E \cdot S + G_X \rightarrow$ Products. To determine whether the metal ion interaction identified in a bacteriophage T4 group I intron (22) is conserved in the *Tetrahymena* group I ribozyme, we measured the effect of Mn^{2+} on the rate of reaction: $E \cdot S + G_{NH_2} \rightarrow$ products $[(k_c/K_m)^{G_{NH_2}}]$. To ensure that the chemical step was rate-determining, the oligonucle-
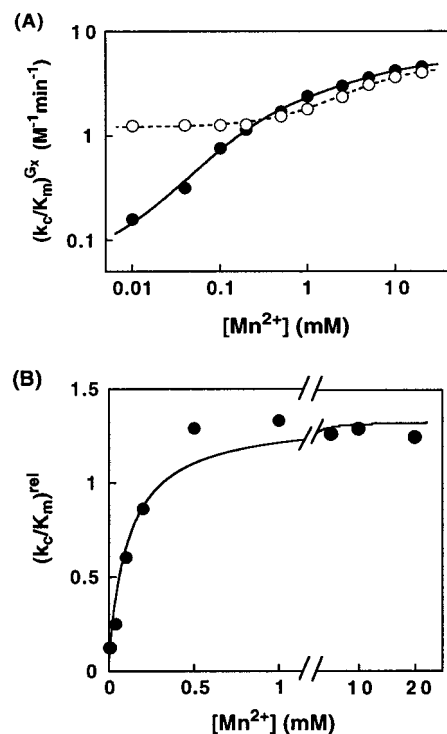

FIGURE 2: (A) Effect of Mn^{2+} on the reaction: $E \cdot S + G_X \rightarrow$ products $[(k_c/K_m)^{G_X}]$ with G_{NH_2} (●) and G (○). $(k_c/K_m)^{G_X}$ was measured in single-turnover reactions with -1d,rSA$_5$ (Chart 1) at pH 7.9, as described under Materials and Methods. The Mn^{2+} effect on the G reaction was fit to a model in which a single Mn^{2+} stimulates the G reaction (dashed line). The data with G_{NH_2} were fit to a model in which the nonspecific Mn^{2+} has the same effect on the G_{NH_2} reaction as on the G reaction and there is an additional Mn^{2+} that specifically stimulates the G_{NH_2} reaction (see text, solid line). (B) Effect of Mn^{2+} on the rate of reaction of G_{NH_2} relative to G: $(k_c/K_m)^{rel} = (k_c/K_m)^{G_{NH_2}}/(k_c/K_m)^G$. The data were fit to eq 6, derived from Scheme 2 (see Materials and Methods), and give an apparent dissociation constant of $K_{E \cdot S}^{Mn,app} = 0.19 \pm 0.04$ mM (10 mM Mg^{2+}) for the Mn^{2+} ion that specifically stimulates the G_{NH_2} reaction.

otide substrate -1d,rSA$_5$ (Chart 1) was used (*38, 49*). Replacing the 2′-OH with a 2′-H at the (−1) position slows the chemical step ∼500-fold, without significant effect on other reaction steps (*40*). Reactions were carried out in a constant background of 10 mM Mg^{2+} to ensure folding of E and to minimize binding of Mn^{2+} to nonspecific metal sites.

Low concentrations of Mn^{2+} (≤1 mM) increase the rate of reaction with G_{NH_2} ∼20-fold, whereas these Mn^{2+} concentrations have no significant effect (<30%) on the analogous reaction with G (Figure 2A). At higher concentrations of Mn^{2+}, the rate of reaction with G increases ∼4-fold. However, the Mn^{2+} effect above 1 mM is similar for reactions of both G_{NH_2} and G, suggesting that the rescue[2] of the reaction of G_{NH_2} is achieved at low Mn^{2+} concentrations and that the Mn^{2+} ion affecting the reaction of G and G_{NH_2} at higher Mn^{2+} concentrations is distinct from the Mn^{2+} ion rescuing the reaction of G_{NH_2}. To isolate the effect of Mn^{2+} that is specific to G_{NH_2}, the rate of reaction of G_{NH_2} relative to G was plotted (Figure 2B). The relative reactivity of G_{NH_2} increases below ∼0.1 mM Mn^{2+} and saturates at higher Mn^{2+} concentration. This Mn^{2+} concentration dependence suggests that a single Mn^{2+} ion binds to $E \cdot S$ and stimulates the reaction of G_{NH_2} (Scheme 2). A fit of the data to the model in Scheme 2 suggests that the Mn^{2+} ion that rescues the

Scheme 1
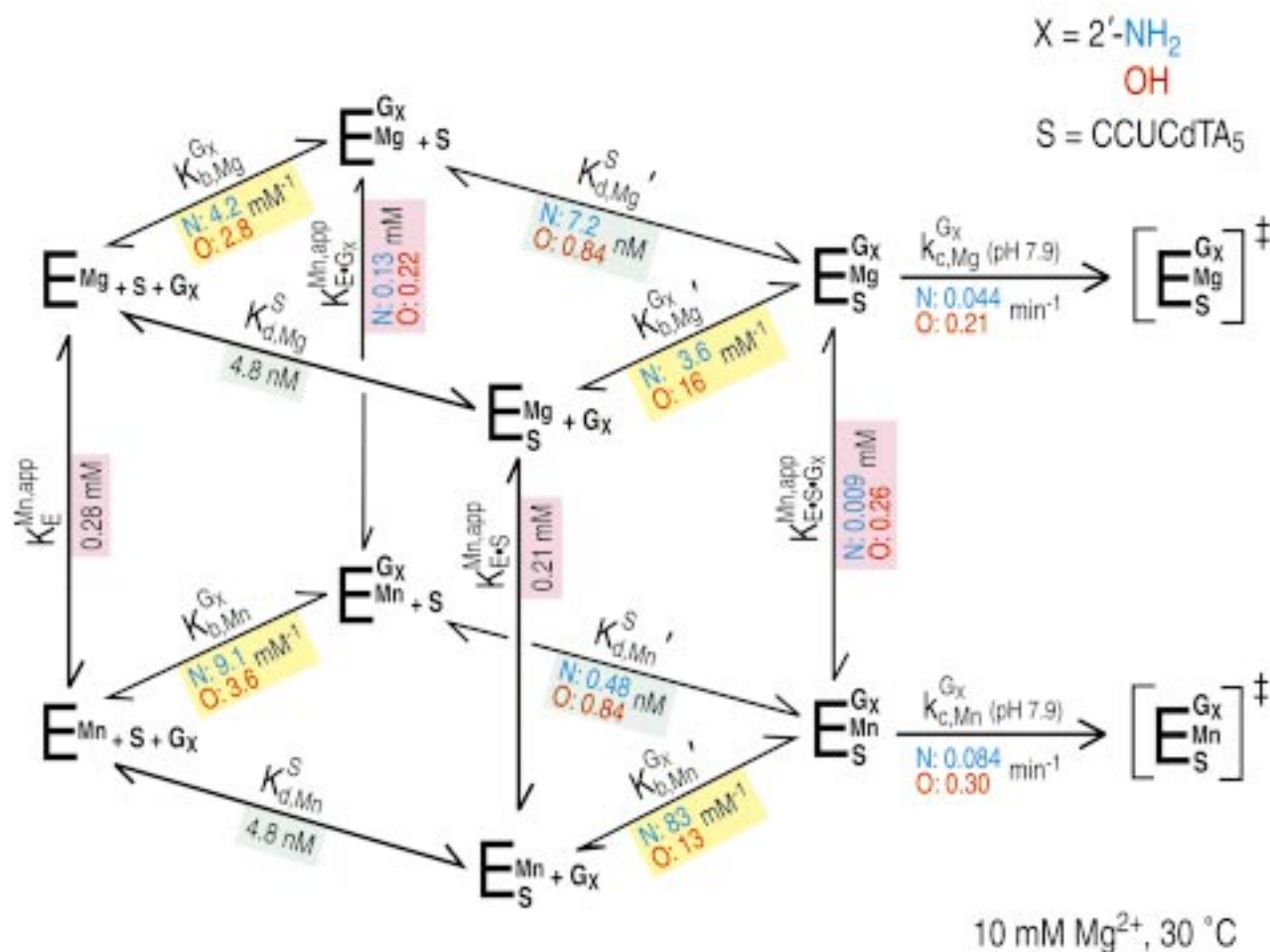
Scheme 2
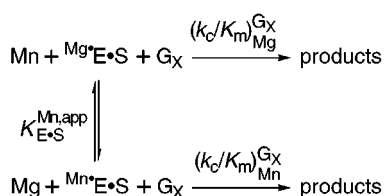
reaction of G_{NH_2} (referred to as Mn_C^{2+}) binds to E·S with an apparent dissociation constant of $K_{E·S}^{Mn,app} = 0.19 \pm 0.04$ mM at 10 mM Mg^{2+}. (This is an apparent equilibrium dissociation constant because Mn_C^{2+} competes with a Mg^{2+} bound at this metal site, as described below.)

Another soft metal ion, Zn^{2+}, also stimulates the reaction of G_{NH_2} ~40-fold at low Zn^{2+} concentrations (0.1 mM), while the effect of Zn^{2+} on the G reaction is only 4-fold (data not shown). Similar rescue of the reaction of G_{NH_2} was observed with the bacteriophage T4 group I intron (*22*). However, saturation of the Zn^{2+} effect on the reactivity of G_{NH_2} could not be obtained, as Zn^{2+} inhibits the ribozyme reaction at higher concentrations under the high pH conditions necessary to follow the reaction of G_{NH_2}. For this reason, we focused on Mn^{2+} in subsequent analyses.

Kinetic and Thermodynamic Framework for the Effect of M_C on Individual Steps of the Tetrahymena Ribozyme Reaction. The results of the previous section provide strong evidence for a direct Mn^{2+} interaction with the 2′-moiety of

G_{NH_2} in the transition state of the *Tetrahymena* ribozyme reaction (Figure 1, M_C). To further understand the role of this metal ion interaction in catalysis by the *Tetrahymena* ribozyme, the individual reaction steps affected by Mn_C^{2+} were identified, and the magnitudes of the effects were quantitated. The thermodynamic and kinetic framework in Scheme 1 summarizes the results of this analysis and provides a guide for the description in this section. Scheme 1 depicts four thermodynamic and kinetic schemes for the ribozyme reaction. The top plane depicts reactions with Mg^{2+} bound at site C, and the bottom plane depicts reactions with Mn^{2+} bound. In each of these planes, reaction schemes for both G and G_{NH_2} are presented, with the individual rate and equilibrium constants for G shown in red and those for G_{NH_2} in blue; the rate and equilibrium constants that are independent of G and G_{NH_2} are shown in black. Each reaction scheme includes the equilibrium constants for binding of G_X to E and E·S ($K_b^{G_X}$ and $K_b^{G_X\prime}$, respectively[3]), the equilibrium constants for dissociation of S from E·S and E·S·G_X (K_d^S and $K_d^{S\prime}$, respectively), and the rate constant of chemical step for the E·S·G_X ternary complex ($k_c^{G_X}$).[4] The identity of the metal ion bound at site C is denoted by a subscript Mn or Mg in the rate and equilibrium constants. The vertical arrows that connect the top and bottom planes represent the equilibrium dissociation constant of Mn^{2+} from site C ($K^{Mn,app}$),[4] with the superscript 'app' denoting that the values reported are apparent dissociation constants of Mn_C^{2+} in the

presence of 10 mM Mg^{2+}. The actual affinity is higher, as Mn_C^{2+} competes with a Mg^{2+} bound at this site. The subscript accompanying the Mn^{2+} dissociation constants depicts the ribozyme or ribozyme·substrate species (e.g., $K_{E\cdot S}^{Mn,app}$ represents the dissociation constant of Mn_C^{2+} from the E·S complex).

With the exception of $K_{E\cdot S}^{Mn,app}$ and $K_{E\cdot S\cdot G}^{Mn,app}$, each rate and equilibrium constant in Scheme 1 was directly determined and, in several cases, determined by two independent experimental methods. The values of $K_{E\cdot G}^{Mn,app}$ and $K_{E\cdot S\cdot G}^{Mn,app}$ were calculated from the thermodynamic relationships in Scheme 1, as Mn^{2+} does not affect the binding of G (see below).

The effect of Mn_C^{2+} on individual reaction steps is described in the following order: (A) the binding of G_{NH_2} to the E·S complex ($K_b^{G_{NH_2}'}$); (B) the binding of G_{NH_2} to free E ($K_b^{G_{NH_2}}$); (C) the affinity of S for the E and E·G_X complexes (K_d^S and $K_d^{S'}$); and (D) the chemical step ($k_c^{G_X}$). Evidence that Mn_C^{2+} competes with a Mg^{2+} bound at site C is presented at the end of this section (E).

(A) A Mn^{2+} Ion Increases the Binding of G_{NH_2} to the E·S Complex. Equilibrium constants for binding of G_{NH_2} and G to the E·S complex (Scheme 3, $K_b^{G_X}$)[3] were determined at varying Mn^{2+} concentrations.

Scheme 3

$$K_b^{G_X}$$
$$E(\cdot S) + G_X \rightleftharpoons E(\cdot S)\cdot G_X$$

$$K_b^{G_X} = 1/K_d^{G_X} = \frac{[E(\cdot S)\cdot G_X]}{[E(\cdot S)][G_X]}$$
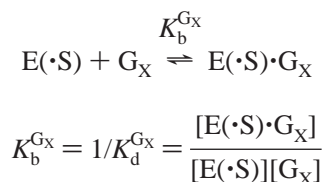
The binding of G_{NH_2} to E·S is strengthened as Mn^{2+} is increased (Figure 3A). In contrast, the binding of G is the same, within error, with or without added Mn^{2+} (Figure 3B). The binding constant of G_{NH_2} as a function of Mn^{2+} concentration follows the dependence predicted for a single Mn^{2+} ion, as described by Scheme 4[5] (Figure 3C). It was not necessary to correct for the effect of Mn^{2+} on the binding of G, as Mn^{2+} does not affect G binding. The fit of the data according to Scheme 4 suggests that the Mn^{2+} ion that increases the binding of G_{NH_2} binds to the E·S complex with $K_{E\cdot S}^{Mn,app} = 0.21 \pm 0.02$ mM at 10 mM Mg^{2+} (Figure 3C, solid line). This is the same, within error, as the dissociation constant of Mn_C^{2+} determined independently ($K_{E\cdot S}^{Mn,app} = 0.19$ mM; Figure 2). The agreement of the Mn^{2+} affinities suggests that the same Mn^{2+} ion, Mn_C^{2+}, is responsible for increasing the binding of G_{NH_2} to E·S.

---

[3] The Mn^{2+} concentration dependence of the binding constant, $K_b^{G_{NH_2}}$, is reported instead of the dissociation constant, $K_d^{G_{NH_2}}$, for convenience in plotting and describing the results. Analysis of the Mn^{2+} concentration dependence of either $K_b^{G_{NH_2}}$ or $K_d^{G_{NH_2}}$, in conjunction with the magnitude of the Mn^{2+} effect, gives the affinity of Mn_C^{2+} for both E·S and E·S·G_{NH_2}. However, the plot of $K_b^{G_{NH_2}}$ versus Mn^{2+} concentration directly gives the dissociation constant of Mn_C^{2+} from E·S (*1*).

[4] Two significant figures are reported for the rate and equilibrium constants in Scheme 1 and Table 1 to help the reader follow the thermodynamic calculations under Results. These rate and equilibrium constants are accurate to only one significant figure, however, based on estimates of experimental error from the range of values obtained in independent experiments.
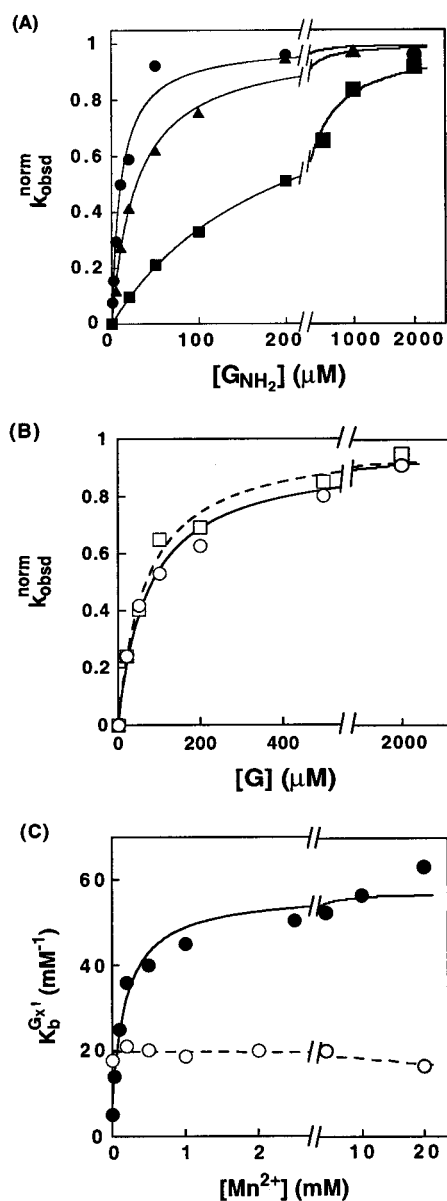

FIGURE 3: Effect of Mn^{2+} on the binding of G and G_{NH_2} to the E·S complex. (A) G_{NH_2} concentration dependence of the observed rate constants (k_{obsd}) for reaction of -1d,rSA5 (Chart 1) at pH 7.9 with E saturating with respect to S at 0 (■), 0.2 mM (▲), and 20 mM Mn^{2+} (●) (see Materials and Methods). The rate constants were normalized such that $k_{obsd}^{norm} = 1$ with saturating G_{NH_2}. The lines are fits of the data to eq 2 and give dissociation constants for G_{NH_2} of 280, 29, and 12 μM at 0, 0.2, and 20 mM Mn^{2+}, respectively. (B) G concentration dependence of the observed rate constants determined under the same conditions as in part A with 0 (○) and 20 mM Mn^{2+} (□). The lines are fits of the data to eq 2 and give dissociation constants for G of 63 and 77 μM at 0 and 20 mM Mn^{2+}, respectively. (C) Effect of Mn^{2+} on the binding constants of G_{NH_2} (●) and G (○), $K_b^{G_X'}$. Values of $K_b^{G_X'}$ were determined in parts A and B and analogous experiments. The data with G_{NH_2} were fit to eq 7, derived from Scheme 4 (solid line; see Materials and Methods), and give $K_{E\cdot S}^{Mn,app} = 0.21 \pm 0.02$ mM (10 mM Mg^{2+}). The dashed line indicates that Mn^{2+} has no significant effect on the binding of G.

The data in Figure 3C also give the affinities of G_{NH_2} for E·S at zero and saturating Mn^{2+} concentrations, with $K_{b,Mg}^{G_{NH_2}'} = 3.6$ mM^{-1} and $K_{b,Mn}^{G_{NH_2}'} = 83$ mM^{-1}, respectively. The affinity of Mn_C^{2+} for E·S·G_{NH_2} can then be calculated from the ~20-fold increase in the binding of G_{NH_2} and the affinity

Scheme 4
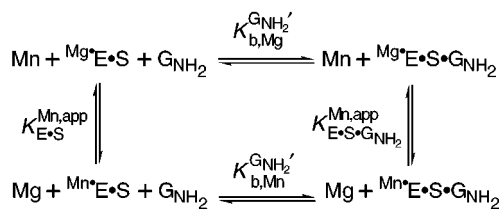
Scheme 5
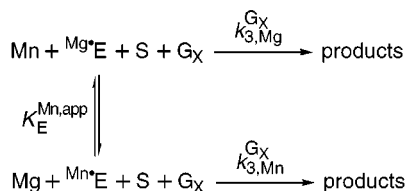
of Mn_C^{2+} for E·S, yielding an apparent dissociation constant of $K_{E \cdot S \cdot G_{NH_2}}^{Mn,app} = 9 \ \mu M$ [10 mM Mg^{2+}; from $K_{E \cdot S \cdot G_{NH_2}}^{Mn,app} = (K_{b,Mg}^{G_{NH_2}'}/K_{b,Mn}^{G_{NH_2}'}) \times K_{E \cdot S}^{Mn,app} = (3.6/83) \times 0.21$ mM $= 0.009$ mM].

In contrast, the data in Figure 3B,C suggest that the binding of G to E·S is not affected by Mn_C^{2+}, with $K_{b,Mg}^{G'} = 16$ mM^{-1} and $K_{b,Mn}^{G'} = 13$ mM^{-1}, respectively, when Mg^{2+} or Mn^{2+} occupies metal site C (Scheme 1). Thus, the affinity of Mn_C^{2+} for E·S·G is essentially the same as that for E·S, with an apparent dissociation constant of $K_{E \cdot S \cdot G}^{Mn,app} = 0.26$ mM [from $K_{E \cdot S \cdot G}^{Mn,app} = (K_{b,Mg}^{G'}/K_{b,Mn}^{G'}) \times K_{E \cdot S}^{Mn,app} = (16/13) \times 0.21$ mM $= 0.26$ mM].

(B) Mn^{2+} Has Little or No Effect on the Binding of G_{NH_2} to Free E. In contrast to the 20-fold increase in the binding of G_{NH_2} to E·S upon addition of Mn^{2+}, added Mn^{2+} has at most a small effect on the binding of G_{NH_2} to free E, with observed binding constants of 4.2 and 9.1 mM^{-1} with 0 and 20 mM Mn^{2+}, respectively (data not shown). The binding of G to free E is also not significantly affected by Mn^{2+}, with binding constants of 2.8 and 3.6 mM^{-1} with 0 and 20 mM Mn^{2+}, respectively (data not shown).

Two models could account for the absence of a Mn^{2+} effect on the binding of G_{NH_2} to E. (1) Mn^{2+} can bind and saturate site C in free E, but does not contribute to the binding of G_{NH_2} in the absence of bound S. (2) Mn_C^{2+} may bind very weakly to free E, with a dissociation constant above 20 mM, thereby obscuring an effect of Mn_C^{2+} on G_{NH_2} binding. To differentiate between these models, the affinity of Mn_C^{2+} for free E was determined by following the Mn^{2+} concentration dependence of the reactivity of G_{NH_2} relative to G in the reaction: E + S + G_X → products ($k_3^{G_X}$; Scheme 5). This is possible because Mn_C^{2+} selectively increases the reactivity of G_{NH_2}, as described above.

Figure 4A shows the effect of Mn^{2+} on the reaction: E + S + G_X → products. Mn^{2+} increases the rate of reaction of G_{NH_2} ~200-fold, whereas the effect on the G reaction is only ~20-fold. Above 1 mM Mn^{2+}, the reaction rates of G_{NH_2} and G are within 2-fold of one another, indicating that the rescue is achieved at lower Mn^{2+} concentrations and that the effects of Mn^{2+} on the reactions of G_{NH_2} and G are from an additional Mn^{2+} ion(s) distinct from Mn_C^{2+}.[6] As described with Figure 2 above, the increased reactivity of G_{NH_2}, relative to G, is expected to follow the concentration
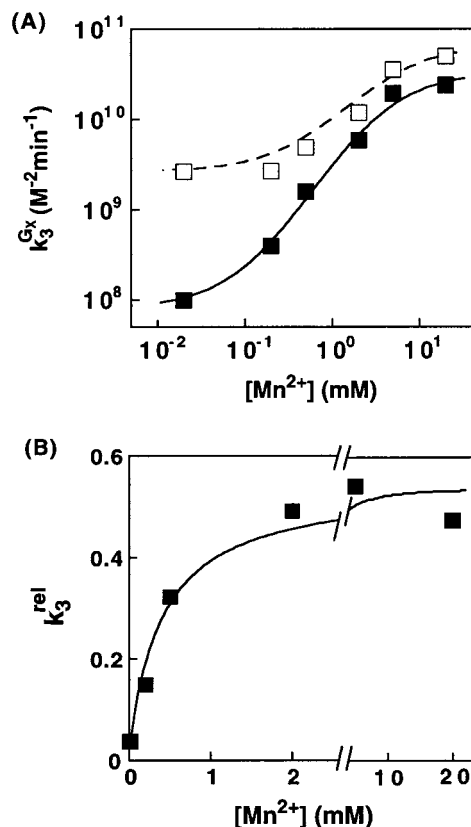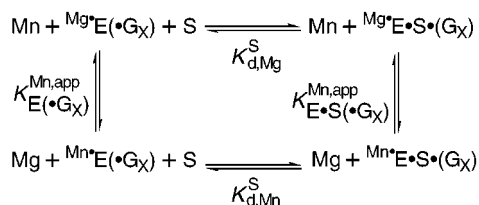
FIGURE 4: (A) Effect of Mn^{2+} on the reactivity of G_{NH_2} (■) and G (□) in the reaction: E + S + G_X → products ($k_3^{G_X}$). $k_3^{G_X}$ was measured in single-turnover reactions with dSA_5 (Chart 1) at pH 7.9, as described under Materials and Methods. The data with G were fit to a model in which a single Mn^{2+} stimulates the G reaction (dashed line). The data with G_{NH_2} were fit to a model in which this Mn^{2+} has the same effect on the G_{NH_2} reaction as on the G reaction, and there is an additional Mn^{2+} that specifically increases the reactivity of G_{NH_2} (solid line). (B) Effect of Mn^{2+} on the rate of reaction of G_{NH_2} relative to G: $k_3^{rel} = k_3^{G_{NH_2}}/k_3^G$. The data were fit to eq 8, derived from Scheme 5 (see Materials and Methods), and give $K_E^{Mn,app} = 0.28 \pm 0.06$ mM (10 mM Mg^{2+}) for binding of the Mn^{2+} that specifically rescues the reaction of G_{NH_2}.

dependence for binding of Mn_C^{2+} (Figure 4B). The Mn^{2+} concentration dependence of the relative reactivity of G_{NH_2} suggests that Mn_C^{2+} binds to E with a dissociation constant of $K_E^{Mn,app} = 0.28 \pm 0.06$ mM and specifically stimulates the G_{NH_2} reaction (Scheme 5). Thus, Mn_C^{2+} saturates free E well below 20 mM but does not significantly enhance the binding of G_{NH_2} [model (1) above].

Placing these results in the context of Scheme 1, Mn_C^{2+} binds to free E with an apparent dissociation constant of $K_E^{Mn,app} = 0.28$ mM. In the absence of S, the Mn^{2+} bound at site C does not interact strongly with G_{NH_2}, with a less than 3-fold effect on the binding of G_{NH_2} to E ($K_{b,Mg}^{G_{NH_2}} = 4.2$ mM^{-1} and $K_{b,Mn}^{G_{NH_2}} = 9.1$ mM^{-1}). This small increase in the affinity of G_{NH_2} upon binding of Mn^{2+} to site C gives an affinity of Mn_C^{2+} for the E·G_{NH_2} complex that is slightly higher than that for free E, with an apparent dissociation constant of $K_{E \cdot G_{NH_2}}^{Mn,app} = 0.13$ mM [$K_{E \cdot G_{NH_2}}^{Mn,app} = (K_{b,Mg}^{G_{NH_2}}/K_{b,Mn}^{G_{NH_2}}) \times$

Scheme 6

$$Mn + {}^{Mg\bullet}E(\bullet G_X) + S \xrightleftharpoons[K^S_{d,Mg}]{} Mn + {}^{Mg\bullet}E\bullet S\bullet(G_X)$$

$$K^{Mn,app}_{E(\bullet G_X)} \Updownarrow \qquad\qquad K^{Mn,app}_{E\bullet S\bullet(\bullet G_X)} \Updownarrow$$

$$Mg + {}^{Mn\bullet}E(\bullet G_X) + S \xrightleftharpoons[K^S_{d,Mn}]{} Mg + {}^{Mn\bullet}E\bullet S\bullet(G_X)$$

$K^{Mn,app}_E = (4.2/9.1) \times 0.28$ mM $= 0.13$ mM]. Mn^{2+}_C does not significantly affect the binding of G to E either ($K^G_{b,Mg} = 2.8$ mM^{-1} and $K^G_{b,Mn} = 3.6$ mM^{-1}). Therefore, the affinity of Mn^{2+}_C for the E·G complex is essentially the same as that for E, with a dissociation constant of $K^{Mn,app}_{E\cdot G} = 0.22$ mM [$K^{Mn,app}_{E\cdot G} = (K^G_{b,Mg}/K^G_{b,Mn}) \times K^{Mn,app}_E = (2.8/3.6) \times 0.28$ mM $= 0.22$ mM].

(C) Mn^{2+}_C Increases the Binding of S to $E\cdot G_{NH_2}$. The ability of Mn^{2+}_C to increase the binding of G_{NH_2} to the E·S complex but not to free E suggests that there is energetic communication between the oligonucleotide substrate and Mn^{2+}_C. To provide an independent test for this communication, the effect of Mn^{2+}_C on the binding of S was investigated (Scheme 6).[5]

Figure 5A shows that Mn^{2+} strengthens the binding of S to the $E\cdot G_{NH_2}$ complex, decreasing the dissociation constant of S from $E\cdot S\cdot G_{NH_2}$ 180-fold. In contrast, Mn^{2+} has only a ~10-fold effect on the dissociation of S from E·S or E·S·G (open symbols). Further, the effect of Mn^{2+} on the binding of S is similar above 0.2 mM, indicating that the preferential strengthening of the binding of S to $E\cdot G_{NH_2}$ is achieved at lower Mn^{2+} concentrations. As described above, the effect of Mn^{2+} on S binding that is specific to bound G_{NH_2} was isolated by plotting the dissociation constant of S from $E\cdot S\cdot G_{NH_2}$ relative to that from E·S·G (Figure 5B, $K^{S,rel}_d$). The value of $K^{S,rel}_d$ follows the Mn^{2+} concentration dependence for a single Mn^{2+} and gives an apparent dissociation constant of $K^{Mn,app}_{E\cdot S\cdot G_{NH_2}} = 10 \pm 2$ μM (Scheme 6; 10 mM Mg^{2+}). This is the same, within error, as the value of 9 μM determined above from the increased binding of G_{NH_2} to E·S by Mn^{2+} (Scheme 1, $K^{Mn,app}_{E\cdot S\cdot G_{NH_2}}$), providing strong evidence that Mn^{2+}_C strengthens the binding of S to $E\cdot G_{NH_2}$.

The effect of Mn^{2+} on the binding of S to E and E·G is not caused by Mn^{2+}_C. Because Mn^{2+}_C has similar affinities for E and E·S (and also the E·G and E·G·S complexes), the thermodynamic cycle of Scheme 6 predicts that the binding of S to E (or to E·G) would not be affected by the binding of Mn^{2+}_C:

$$\frac{K^S_{d,Mn}}{K^S_{d,Mg}} = \frac{K^{Mn,app}_{E\cdot S}}{K^{Mn,app}_E} = \frac{0.21}{0.28} \approx 1$$

and

$$\frac{K^S_{d,Mn}{}'}{K^S_{d,Mg}{}'} = \frac{K^{Mn,app}_{E\cdot S\cdot G}}{K^{Mn,app}_{E\cdot G}} = \frac{0.26}{0.22} \approx 1$$

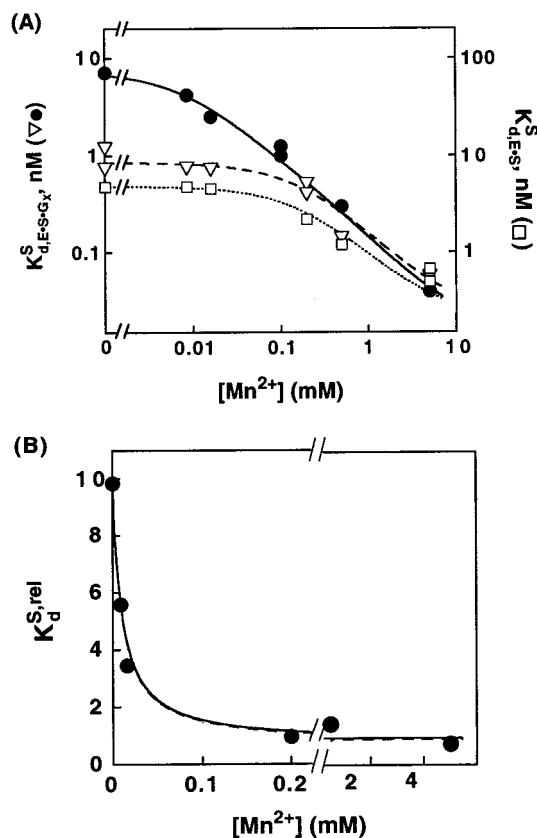(values from Scheme 1). This conclusion was confirmed by independent experiments that showed that the effect of Mn^{2+}

FIGURE 5: (A) Effect of Mn^{2+} on the dissociation constant of S from E·S ($\square$, $K^S_{d,E\cdot S}$), E·S·G ($\triangledown$, $K^S_{d,E\cdot S\cdot G}$), and $E\cdot S\cdot G_{NH_2}$ ($\bullet$, $K^S_{d,E\cdot S\cdot G_{NH_2}}$). Dissociation constants of S were determined with CCUCdTA$_5$ by both equilibrium binding and pulse–chase experiments, as described under Materials and Methods. The effects of Mn^{2+} on the dissociation of S from E·S and E·S·G are from a Mn^{2+} ion that is distinct from the Mn^{2+} ion that specifically decreases the dissociation constant of S from $E\cdot S\cdot G_{NH_2}$ and were fit to a model for an effect from a single Mn^{2+} ion (dashed and dotted lines; see text).[6] The solid line shows a fit of the $E\cdot S\cdot G_{NH_2}$ data to a model in which this Mn^{2+} has the same effect on the dissociation of S from $E\cdot S\cdot G_{NH_2}$ as from the E·S(·G) complexes and there is an additional Mn^{2+} ion that specifically decreases the dissociation constant of S from $E\cdot S\cdot G_{NH_2}$ (see text). (B) Effect of Mn^{2+} on the dissociation of S from $E\cdot S\cdot G_{NH_2}$ relative to that from E·S·G: $K^{S,rel}_d = K^S_{d,E\cdot S\cdot G_{NH_2}}/K^S_{d,E\cdot S\cdot G}$. The data were fit to eq 10, derived from Scheme 6 (solid line; see Materials and Methods), and give $K^{Mn,app}_{E\cdot S\cdot G_{NH_2}} = 10 \pm 2$ μM (10 mM Mg^{2+}) for the Mn^{2+} ion that specifically increases the affinity of S in the presence of bound G_{NH_2}. The dashed line (barely visible) is a theoretical curve for the effect predicted for Mn^{2+}_C, calculated from values determined in independent experiments: $K^{Mn,app}_{E\cdot S\cdot G_{NH_2}} = 9$ μM (Figure 3) and a 12-fold increase in S binding upon binding of Mn^{2+}_C [from the 23-fold versus ~2-fold effect of Mn^{2+}_C on the binding of G_{NH_2} to E·S and to free E, respectively (Figure 3 and data not shown), and the thermodynamic cycle of Scheme 6].

on the binding of S to E (or E·G) stems from a Mn^{2+} ion distinct from Mn^{2+}_C that interacts with the A(+1) residue of S (Chart 1).[6] Thus, the 18-fold larger effect of Mn^{2+} on the

---

[6] The Mn^{2+} effect on the binding of S to E(·G) was eliminated when A(+1) was replaced by a methyl group (rS$_{Me}$, Chart 1), whereas this substitution has no effect on the ability of Mn^{2+}_C to rescue the binding and reaction of G_{NH_2} (unpublished results). These experiments strongly suggest that the additional Mn^{2+} effect on S binding stems from a distinct Mn^{2+} ion that interacts with A(+1) and, further, that the effects of Mn^{2+}_C and this additional Mn^{2+} ion are independent of one another.

binding of S to $E \cdot G_{NH_2}$ relative to free E and $E \cdot G$ (Figure 5A) represents the effect that stems from Mn_C^{2+}, and the remaining effect that is common to G and G_{NH_2} arises from a distinct Mn^{2+} ion.

Placing these results in the context of Scheme 1, Mn_C^{2+} strengthens the binding of S to the $E \cdot G_{NH_2}$ complex, decreasing the dissociation constant of S 18-fold, from $K_{d,Mg}^{S\prime} = 7.2$ nM to $K_{d,Mg}^{S\prime} = 0.48$ nM ($K_{d,Mn}^{S\prime} = K_{d,Mg}^{S\prime}/18 = 7.2$ nM$/18 = 0.48$ nM; blue numbers for G_{NH_2}). In contrast, the affinities of S for E and $E \cdot G$ are not significantly affected by Mn_C^{2+}. The dissociation constants of S from $E \cdot S$ and $E \cdot S \cdot G$ are the same regardless of whether a Mg^{2+} or a Mn^{2+} is bound at site C, with $K_{d,Mg}^S = K_{d,Mn}^S = 4.8$ nM and $K_{d,Mg}^{S\prime} = K_{d,Mn}^{S\prime} = 0.84$ nM (red numbers for G).

(D) Effect of Mn_C^{2+} on the Chemical Step. Addition of 1 mM Mn_C^{2+} to the $E \cdot S \cdot G_{NH_2}$ complex, which is more than 100-fold above the dissociation constant for Mn_C^{2+} (Scheme 1, $K_{E \cdot S \cdot G_{NH_2}}^{Mn,app} = 9$ μM), does not significantly affect the rate of the chemical step with G_{NH_2}. The rate constants with and without added Mn^{2+} are $k_{c,Mn}^{G_{NH_2}} = 0.084$ min^{-1} and $k_{c,Mg}^{G_{NH_2}} = 0.044$ min^{-1}, respectively (pH 7.9; Scheme 1; data not shown). The rate of the chemical step with G is also not significantly affected by addition of 1 mM Mn^{2+}, which is 5-fold above the dissociation constant for Mn_C^{2+} from $E \cdot S \cdot G$ (pH 7.9; Scheme 1, $k_{c,Mn}^G = 0.30$ min^{-1} and $k_{c,Mg}^G = 0.21$ min^{-1}; data not shown). Thus, Mn_C^{2+} has no significant effect on the reaction of G_{NH_2} from the ternary complex, $E \cdot S \cdot G_{NH_2}$.

(E) Mn_C^{2+} Competes with a Mg^{2+} Ion Bound at Site C. If metal site C is unoccupied, then the Mn_C^{2+} affinity would not be affected by changes in the Mg^{2+} concentration, provided that sufficient Mg^{2+} is present to fold the ribozyme (≥ 2 mM Mg^{2+} used herein; refs 6, 50, 51). Alternatively, if Mg^{2+} occupies site C at the concentrations required for folding, then Mn^{2+} must compete with this Mg^{2+} ion, and the observed affinity of Mn_C^{2+} would decrease with increasing [Mg^{2+}]. The results described in this section strongly suggest that a Mg^{2+} ion occupies site C in the free ribozyme and in all of the ribozyme·substrate complexes.

For E and $E \cdot S$, this was ascertained by determining the apparent affinity of Mn_C^{2+} at various Mg^{2+} concentrations by experiments analogous to those presented in Figures 3C and 4 above. The apparent affinities of Mn_C^{2+} for $E \cdot S$ were obtained from Figure 6; these data and those for E (Figure 4 and data not shown) are summarized in Table 1. The apparent affinities of Mn_C^{2+} for both E and $E \cdot S$ decrease linearly as [Mg^{2+}] is increased from 2 to 50 mM. These results are consistent with predictions from competitive binding of Mn_C^{2+} with Mg_C^{2+} and suggest that the dissociation constant for binding of Mg_C^{2+} to free E and the $E \cdot S$ complex is less than 2 mM. Also, the high apparent affinity of Mn_C^{2+} at each Mg^{2+} concentration suggests that Mn^{2+} binds ~40–50-fold more strongly than Mg^{2+} to site C in free E and the $E \cdot S$ complex (Table 1, K_E^{rel} and $K_{E \cdot S}^{rel}$).

The observed affinity of Mn_C^{2+} for $E \cdot S$ at individual Mg^{2+} concentrations (Table 1, $K_{E \cdot S}^{Mn,app}$) and the increase of ~20-fold in the affinity of G_{NH_2} upon binding of Mn_C^{2+} at each Mg^{2+} concentration also allowed calculation of the apparent affinity of Mn_C^{2+} for the $E \cdot S \cdot G_{NH_2}$ complex at each
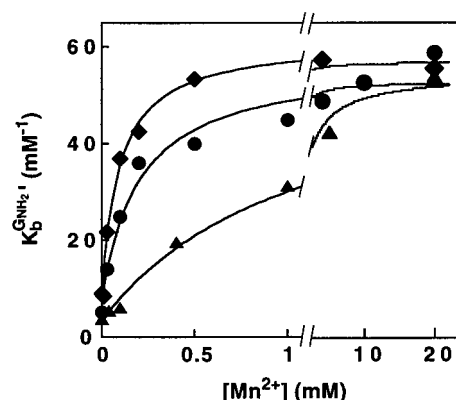

FIGURE 6: Mn^{2+} concentration dependence of the binding of G_{NH_2} to $E \cdot S$ at 2 (◆), 10 (●), and 50 mM Mg^{2+} (▲), $K_b^{G_{NH_2}\prime}$, determined as described in Figure 3C. The data at 10 mM Mg^{2+} are from Figure 3C and are shown for comparison. The Mn^{2+} concentration dependence at each Mg^{2+} concentration were fit to eq 7, derived from Scheme 4, and give $K_{E \cdot S}^{Mn,app} = 0.044 \pm 0.05$ and 1.1 ± 0.1 mM at 2 and 50 mM Mg^{2+}, respectively.

Table 1: Mn_C^{2+} Competes with a Mg^{2+} for Binding to Metal Site C

[Mg^{2+}] (mM)	$K_E^{Mn,app\ a}$ (mM)	$K_E^{rel\ b}$	$K_{E \cdot S}^{Mn,app\ c}$ (mM)	$K_{E \cdot S}^{rel\ b}$	$K_{E \cdot S \cdot GNH_2}^{Mn,app\ d}$ (mM)	$K_E^{rel\ b}$
2	0.058	35	0.044	45	0.0019	1100
10	0.28	37	0.21	47	0.0090	1100
50	1.3	38	1.1	46	0.048	1000

[a] Observed dissociation constant of Mn_C^{2+} from E at each Mg^{2+} concentration, determined from the Mn^{2+} concentration dependence of the relative reactivity of G_{NH_2} in the reaction: $E + S + G_X \rightarrow$ products as described under Materials and Methods (Figure 4 and data not shown). [b] $K^{rel} \approx$ [Mg^{2+}]$/K^{Mn,app}$, and gives the specificity of metal site C for Mn^{2+} relative to Mg^{2+} as described under Materials and Methods. The subscript accompanying the K^{rel} values denotes the ribozyme or ribozyme·substrate complex that binds Mn^{2+} at site C. [c] Observed dissociation constant of Mn_C^{2+} from $E \cdot S$ at each Mg^{2+} concentration (from Figure 6). [d] Apparent dissociation constant of Mn_C^{2+} from $E \cdot S \cdot G_{NH_2}$ at each Mg^{2+} concentration, calculated from the following thermodynamic relationship in Scheme 4: $K_{E \cdot S \cdot G_{NH_2}}^{Mn,app} = (K_{b,Mg}^{G_{NH_2}\prime}/K_{b,Mn}^{G_{NH_2}\prime}) \times K_{E \cdot S}^{Mn,app}$. The value of $K_{E \cdot S}^{Mn,app}$ at each Mg^{2+} concentration is from this table, and $K_{b,Mg}^{G_{NH_2}\prime}$ and $K_{b,Mn}^{G_{NH_2}\prime}$ are the binding constants of G_{NH_2} with zero and saturating Mn^{2+} in Figure 6, respectively.

Mg^{2+} concentration, as described in Table 1 ($K_{E \cdot S \cdot G_{NH_2}}^{Mn,app}$). These apparent affinities and the observed competition of Mn_C^{2+} with Mg^{2+} then allowed calculation of the Mn^{2+} specificity of site C in the $E \cdot S \cdot G_{NH_2}$ complex, as also described in Table 1 ($K_{E \cdot S \cdot G_{NH_2}}^{rel}$). These calculations strongly suggest that Mn^{2+} binds ~1000-fold stronger than Mg^{2+} to site C in the $E \cdot S \cdot G_{NH_2}$ complex, with an upper limit of 2 μM for the dissociation constant of Mn_C^{2+}, obtained from its apparent dissociation constant at the lowest Mg^{2+} concentration investigated.

The absence of a Mg^{2+} concentration effect on the affinity of G or G_{NH_2} for E($\cdot$S) suggests that Mg^{2+} remains bound at site C in the E($\cdot$S)$\cdot$G and E($\cdot$S)$\cdot G_{NH_2}$ complexes (2–100 mM Mg^{2+}; data not shown). As Mn^{2+} has only a small effect on the binding of G_{NH_2} to free E (data not shown; Scheme 1, $K_{b,Mg}^{G_{NH_2}}$ vs $K_{b,Mn}^{G_{NH_2}}$), the Mn^{2+} affinity and specificity of site C in the $E \cdot G_{NH_2}$ complex are within 2-fold of the values for free E. Analogously, the absence of a Mn^{2+} effect on the binding of G to E and $E \cdot S$ (Figure 3 and data not shown; Scheme 1, $K_{b,Mg}^G$ vs $K_{b,Mn}^G$ and $K_{b,Mg}^{G\prime}$ vs $K_{b,Mn}^{G\prime}$) suggests that
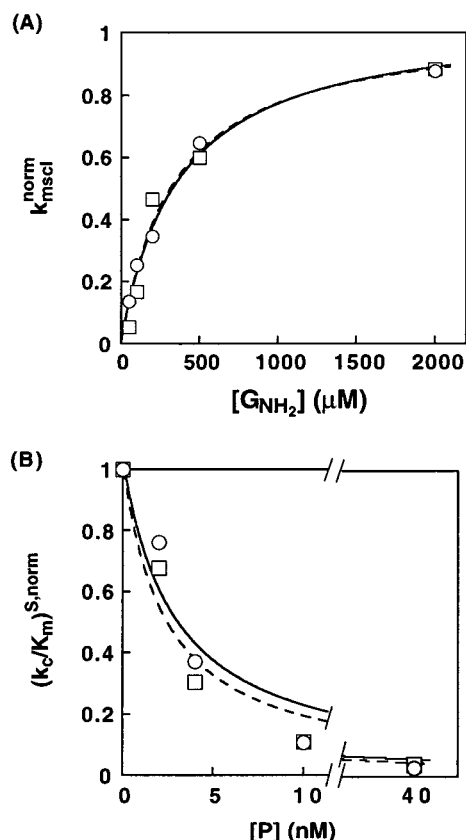
FIGURE 7: (A) G_{NH_2} concentration dependence of the rate of miscleavage of P (k_{mscl}) with zero (○) and 10 mM Mn^{2+} (□) in the presence of 10 mM Mg^{2+}. Single-turnover reactions were carried out at pH 7.9 with trace amounts of labeled oligonucleotide product and excess E to ensure saturation of P (see Materials and Methods). Observed rates of miscleavage were normalized such that $k_{mscl}^{norm} = 1$ with saturating G_{NH_2}. Fits of the data to eq 2 give dissociation constants of 360 and 320 μM for binding of G_{NH_2} to E·P with 0 and 10 mM Mn^{2+}, respectively (dashed and solid lines). (B) Dependence of the rate of the reaction: E·G_{NH_2} + S* → products [$(k_c/K_m)^S$] on the concentration of added inhibitor, CCUCU with zero (○) and 5 mM Mn^{2+} (□), determined in the presence of 10 mM $MgCl_2$ as described in eq 5a under Materials and Methods. $(k_c/K_m)^S$ values were measured with rSA_5 as described under Materials and Methods. Fits of the data to eq 5b, derived from the scheme in eq 5a, give dissociation constants of 2.3 and 2.8 nM, respectively, for binding of CCUCU to E·G_{NH_2} with 0 and 5 mM Mn^{2+}, respectively (dashed and solid lines).

the Mn^{2+} affinity and specificity of site C in the E·G and E·S·G complexes are similar to those for E and E·S.

Effect of the Reactive Phosphoryl Group of S on the Mn_C^{2+}·G_{NH_2} Interaction. In the previous section, we showed that Mn_C^{2+} increases the affinity of G_{NH_2} only when S is bound and that Mn_C^{2+} increases the affinity of S for E·G_{NH_2}. These observations indicate that there is an energetic communication between Mn_C^{2+} and the oligonucleotide substrate. In an effort to identify the group(s) on the oligonucleotide substrate responsible for this communication, we determined the effect of Mn^{2+} on the binding of G_{NH_2} to the ribozyme·oligonucleotide product complex, E·P, in which the reactive phosphoryl group of S is removed and replaced by a hydroxyl group.

The equilibrium constant for binding of G_{NH_2} to E·P was determined by following the rate of miscleavage of P (k_{mscl}) at varying concentrations of G_{NH_2} (see the Materials and Methods). The binding of G_{NH_2} to E·P is the same, within

error, with or without 10 mM Mn^{2+}, with dissociation constants of 320 and 360 μM, respectively (Figure 7A; 10 mM Mg^{2+}). Similar results were obtained from independent experiments in which the affinity of G_{NH_2} for E·P was measured by using G_{NH_2} as an inhibitor of the reverse reaction (see Materials and Methods): dissociation constants for G_{NH_2} of 260 and 280 μM were obtained in the presence and absence of 10 mM Mn^{2+}, respectively (data not shown).

As described above for the case with free E, the absence of a Mn^{2+} effect on the binding of G_{NH_2} to E·P could arise either from weak binding of Mn_C^{2+} to the E·P complex or from the absence of an interaction of G_{NH_2} with bound Mn_C^{2+} in the E·P·G_{NH_2} complex. These two models were distinguished by determining the affinity of Mn_C^{2+} for E·P (cf. Scheme 5 for free E). The binding of Mn_C^{2+} to E·P can be followed as Mn^{2+} provides a 10-fold stimulation of G_{NH_2} in the miscleavage reaction: E·P + G_X → products (see Materials and Methods and ref *43*), but has no effect on miscleavage by G. This observation suggests that the Mn_C^{2+}·G_{NH_2} interaction stimulates the miscleavage reaction, just as it stimulates the normal cleavage reaction. The reactivity of G_{NH_2} in the miscleavage reaction follows the concentration dependence expected for a single Mn^{2+} with an apparent dissociation constant of 0.18 ± 0.06 mM for binding of Mn_C^{2+} to E·P (10 mM Mg^{2+}; data not shown). Thus, Mn^{2+} can bind and saturate metal site C in E·P, but bound Mn_C^{2+} does not interact significantly with G_{NH_2} in the E·P·G_{NH_2} complex. This localizes the communication between Mn_C^{2+} and the oligonucleotide substrate to the reactive phosphoryl group.[6]

In the previous section, we described results that suggest that Mn_C^{2+} increases the affinity of S for the E·G_{NH_2} complex (Figure 5). To provide an independent test of whether the reactive phosphoryl group is required for the interaction of Mn_C^{2+} with S, the effect of Mn^{2+} on the binding of P to the E·G_{NH_2} complex was determined (Figure 7B). In the presence of 5 mM Mn^{2+}, which is 40-fold above the dissociation constant for site C in E·G_{NH_2} (Scheme 1, $K_{E·G_{NH_2}}^{Mn,app} = 0.13$ mM), the affinity of P for the E·G_{NH_2} complex is the same, within error, as the affinity in the absence of Mn^{2+}. This is in contrast to the ~20-fold stronger binding of S to E·G_{NH_2} in the presence of Mn_C^{2+} [Scheme 1, $K_{d,Mg}^S{}'$ vs $K_{d,Mn}^S{}'$ (numbers in blue)] and provides independent evidence that the reactive phosphoryl group of S is responsible for the communication between Mn_C^{2+} and the oligonucleotide substrate.

DISCUSSION

Deciphering the role of individual metal ions in RNA catalysis is an enormous challenge, as a sea of metal ions coat the charged RNA backbone (e.g., *4, 6, 7, 9, 11−13, 16, 19, 52,* and references cited therein). In this work, metal ion specificity switch experiments have been used to identify a metal ion interaction with the 2′-moiety of G in the *Tetrahymena* group I ribozyme (Figure 1, M_C), confirming and extending previous observations in a bacteriophage T4 group I intron (*22*).

The analysis herein relies on comparisons of the effects of Mn^{2+} on the reaction of G_{NH_2} relative to those on the G reaction. Such a comparative approach is crucial for inter-

pretation of the results, as effects of Mn^{2+} that are not specific to the modification on the 2′-moiety of G can often arise from metal ion sites other than site C or from technical problems such as solubility limits of Mn^{2+}. Use of relative reactivities minimizes complications from these nonspecific effects, allowing metal ion effects specific to a single ligand, the 2′-moiety of G, to be quantitatively isolated amidst the sea of metal ions bound to this RNA.
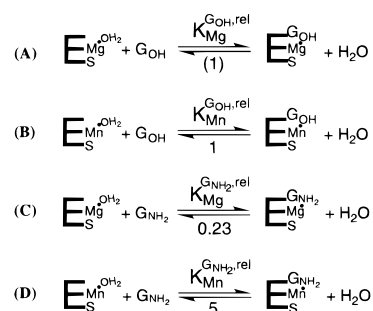
Further, investigation using the well-characterized *Tetrahymena* ribozyme has allowed quantitative analysis of the energetics of the interactions of M_C with the 2′-moiety of G within the ribozyme active site and determination of the affinity and specificity of metal site C in the ribozyme and ribozyme·substrate complexes. The metal ion affinities provide a fingerprint for M_C that allows it to be distinguished from other active site metal ions and have facilitated the isolation of the effect of M_C on individual reaction steps (Scheme 1). The progression of the interactions of M_C along the reaction pathway revealed a communication between M_C and the oligonucleotide substrate. These and other observations suggest that M_C plays an integral role in the coupling of the guanosine nucleophile with the oligonucleotide substrate and possibly in the alignment of the active site.

A Metal Ion Interaction with the 2′-Moiety of G in the Tetrahymena Ribozyme Reaction. Previously, Sjögren et al. observed that self-splicing of a bacteriophage T4 group I intron is ~20-fold slower with G_{NH_2} than with G and that the lower reactivity of G_{NH_2} is rescued by Mn^{2+} and Zn^{2+}, suggesting that there is a metal ion interaction with the 2′-moiety of G in this intron (*22*). An analogous metal ion interaction in the *Tetrahymena* group I ribozyme is suggested by the increased reactivity of G_{NH_2} relative to G by Mn^{2+} and Zn^{2+} observed herein with this ribozyme. In addition, the Mn^{2+} concentration dependences for rescue of the binding and reactivity of G_{NH_2} are as expected for the effect from a single Mn^{2+} ion. These concentration dependences and the low concentration of Mn^{2+} required for rescue (Scheme 1) strongly suggest that the reaction of G_{NH_2} is rescued by a single Mn^{2+} ion. This metal ion is referred to as Mn_C^{2+} herein.

These results provide strong evidence for a direct interaction of Mn^{2+} with the 2′-nitrogen of G_{NH_2} in the transition state of the *Tetrahymena* ribozyme reaction. Direct observation of an interaction of Mg^{2+} at site C with the 2′-OH of G is prevented, however, by the high affinity of metal site C for Mg^{2+} and the requirement of a minimal Mg^{2+} concentration required for folding of this ribozyme (2 mM Mg^{2+} used herein). Nevertheless, an analogous interaction between a Mg^{2+} bound at metal site C and the 2′-OH of G at the ribozyme active site is likely (Figure 1, M_C). The 2′-OH of G contributes more than 10^6-fold to catalysis of the *Tetrahymena* ribozyme relative to a 2′-H (*53, 54,* and unpublished results), and it is difficult to imagine that alternative active site interactions with a 2′-NH_2 substituent could provide the same enormous rate enhancement for the ribozyme reaction. Further, the enormous catalytic contribution of the 2′-OH of G suggests that M_C, the metal ion that coordinates this 2′-OH, may play a crucial role in catalysis (see below).

Energetics of Specific Metal Ion Interactions within Folded RNA. Ribozyme catalysis provides a sensitive probe for binding of functional metal ions to RNA and the energetic
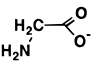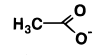
Scheme 7

$$\text{(A)} \quad E_S^{Mg^{OH_2}} + G_{OH} \xrightleftharpoons[(1)]{K_{Mg}^{G_{OH},rel}} E_S^{Mg^{G_{OH}}} + H_2O$$

$$\text{(B)} \quad E_S^{Mn^{OH_2}} + G_{OH} \xrightleftharpoons[1]{K_{Mn}^{G_{OH},rel}} E_S^{Mn^{G_{OH}}} + H_2O$$

$$\text{(C)} \quad E_S^{Mg^{OH_2}} + G_{NH_2} \xrightleftharpoons[0.23]{K_{Mg}^{G_{NH_2},rel}} E_S^{Mg^{G_{NH_2}}} + H_2O$$

$$\text{(D)} \quad E_S^{Mn^{OH_2}} + G_{NH_2} \xrightleftharpoons[5]{K_{Mn}^{G_{NH_2},rel}} E_S^{Mn^{G_{NH_2}}} + H_2O$$
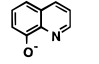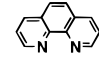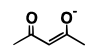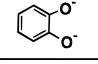
consequences of metal ion−RNA interactions. In this work, the increase in the binding and reactivity of G_{NH_2} upon replacement of the Mg^{2+} at site C with Mn^{2+} has allowed quantitative energetic analysis of the interactions of M_C with the 2′-moiety of G and with the ribozyme active site. Quantitative analyses described below reveal a 20-fold preference for interaction of the 2′-NH_2 group of G_{NH_2} with Mn_C^{2+} relative to Mg_C^{2+}, similar to the preference observed in model compounds. These analyses also indicate that metal site C has a high affinity and specificity for Mn^{2+}, with a dissociation constant of ≤ 2 μM and a preference of 1000-fold relative to Mg^{2+} in the E·S·G_{NH_2} ternary complex.

(A) Energetics of the Metal Ion Interaction with the 2′-Moiety of G. Comparison of the affinities of G and G_{NH_2} with Mg^{2+} or Mn^{2+} bound at metal site C allows quantitative evaluation of the interactions of M_C with the 2′-moiety of G. The results are summarized in Scheme 7, in which equilibrium association constants are shown with superscripts specifying whether the 2′-moiety of G is -OH or -NH_2 and the subscripts specifying whether Mg^{2+} or Mn^{2+} is bound at site C. The equilibrium constants are relative to that for binding of G with Mg^{2+} at site C, so that the value of $K_{Mn}^{G_{OH},rel}$ in part A is defined as equal to 1 ($K_{b,Mg}^{G}{}' = 16$ mM^{-1}; Scheme 1). As only the 2′-substituent of G and the identity of the metal ion bound at site C are varied, these relative affinities isolate the energetics of the interaction of M_C with the 2′-moiety of G in the E·S·G_X complex.

The binding of G with a Mn^{2+} bound at site C is the same, within error, as that with a Mg^{2+} at this site (Scheme 7B, $K_{Mn}^{G_{OH},rel} = K_{b,Mn}^{G}{}'/K_{b,Mg}^{G}{}' = 13/16 \approx 1$; values from Scheme 1). The Mg^{2+} or Mn^{2+} at site C presumably interacts with a water molecule in the absence of bound nucleophile, and this bound water is replaced by the 2′-OH group upon binding of G, as depicted in Scheme 7A,B. Because the 2′-hydroxyl of guanosine is electrostatically similar to the hydroxyl of a water molecule, no effect on intrinsic affinity would be expected. The similar affinities of G with Mg^{2+} or Mn^{2+} bound at site C then suggest that the replacement of Mg^{2+} by Mn^{2+} does not cause a geometrical perturbation of metal site C that compromises binding of guanosine and interaction with its 2′-hydroxyl group.

The stronger binding of G_{NH_2} with Mn^{2+} bound at site C than with Mg^{2+} bound (Scheme 1, $K_{b,Mn}^{G_{NH_2}}{}'$ vs $K_{b,Mg}^{G_{NH_2}}{}'$) presumably reflects the different intrinsic affinities of Mn^{2+} and Mg^{2+} for nitrogen ligands relative to oxygen ligands (*55-57*). With a Mg^{2+} ion occupying site C, the affinity of G_{NH_2} for the E·S complex is ~4-fold lower than that of G, with $K_{Mg}^{G_{NH_2},rel} = 0.23$ (Scheme 7C, $K_{Mg}^{G_{NH_2},rel} = K_{b,Mg}^{G_{NH_2}}{}'/K_{b,Mg}^{G}{}' = 3.6/16 = 0.23$; values from Scheme 1). This suggests that the

Table 2: Equilibrium Constants for Association of Mg^{2+} and Mn^{2+} with Model Compounds

Compound	log K^{M} [a]		K^{rel} [b]	ΔΔG (kcal/mol)[c]
	Mg^{2+}	Mn^{2+}		
(I) NH$_3$	-0.08[d]	1.00[d]	12	-1.51
(II) H$_2$N-CH$_2$CH$_2$-NH$_2$	0.37[d]	2.77[d]	250[e]	-3.36[e]
(III) [H$_2$C—C(=O)—O$^-$, H$_2$N]	1.34	2.80	29	-2.05
(IV) [H$_3$C—C(=O)—O$^-$]	0.55	0.7	1.4	-0.20
(V) [quinolin-8-olate structure]	4.31	6.24	91	-2.74
(VI) [phenanthroline structure]	1.2	4.0	630	-3.92
(VII) OH$^-$	2.58[f]	3.4[f]	6.6	-1.15
(VIII) PO$_4^{3-}$	1.88[g]	2.58[g]	5.0	-0.98
(IX) ATP^{4-}	4.10	4.74	4.4	-0.90
(X) GTP^{4-}	4.08	4.69	4.1	-0.85
(XI) CTP^{4-}	4.04	4.76	5.2	-1.01
(XII) UTP^{4-}	4.01	4.68	4.7	-0.94
(XIII) [dicarboxylate structure]	3.65	4.21	3.6	-0.78
(XIV) [1,2-dihydroxybenzene dianion structure]	5.7	7.72	105	-2.83

[a] K^{M} is the equilibrium association constant for the reaction: M + L ⇌ M·L, in which M is Mg^{2+} or Mn^{2+} and L is the compound that provides ligand(s) for M. Values of K^{M} are in units of M^{-1} and were determined at 25 °C at ionic strength 0.1 unless otherwise specified. From ref 55. [b] $K^{rel} = K^{Mn}/K^{Mg}$, and gives the specificity for association with Mn^{2+} relative to Mg^{2+}. [c] $\Delta\Delta G = -RT \ln K^{rel}$, and gives the difference in binding free energy for Mn^{2+} and Mg^{2+}. Negative values of $\Delta\Delta G$ denote a preference for Mn^{2+}. [d] At ionic strength 0.5. [e] Compound **II** contains two -NH$_2$ groups, so that the free energy difference for each amino group ($\Delta\Delta G'$) is expected to be half of that observed: $\Delta\Delta G' = \Delta\Delta G/2 = -1.68$ kcal/mol. Likewise, $K^{rel'} = \sqrt{K^{rel}} = 16$. [f] At ionic strength 0. [g] At ionic strength 2.0.

interaction of Mn$_C^{2+}$ with the 2′-NH$_2$ of G is 4-fold weaker than with 2′-OH. In contrast, the affinity of G$_{NH_2}$ with Mn^{2+} at site C is ∼5-fold higher than that of G (Scheme 7D, $K_{Mn}^{G_{NH_2},rel} = K_{b,Mn}^{G_{NH_2}'}/K_{b,Mg}^{G'} = 83/16 ≈ 5$; values from Scheme 1), suggesting that the interaction of Mn$_C^{2+}$ with the 2′-NH$_2$ of G is 5-fold stronger than with 2′-OH. Combining these observations, G$_{NH_2}$ binds 20-fold stronger with Mn^{2+} bound at site C than with Mg^{2+} bound (Scheme 7C,D). This corresponds to a 1.8 kcal/mol preference of Mn^{2+} over Mg^{2+} for interaction with the 2′-NH$_2$ group, relative to interaction with a water ligand. This preference is similar to those observed with several model compounds, which give free energy preferences of 1.5-2.1 kcal/mol for interaction with each amino group (Table 2, compounds **I**−**III**).

(B) Affinity and Specificity of Metal Site C. Quantitative analysis of the Mn^{2+} concentration dependence of the binding or reaction of G$_{NH_2}$ allowed determination of the affinity of metal site C for Mn^{2+} and Mg^{2+} in the ribozyme and ribozyme·substrate complexes (Scheme 1 and Table 1). This analysis indicates that site C has a high affinity and specificity for Mn^{2+}. Even in the absence of bound G$_{NH_2}$, Mn$_C^{2+}$ binds 50-fold stronger than Mg$_C^{2+}$, with a dissociation constant of ≤40 μM for unoccupied site C (Table 1). In the E·S·G$_{NH_2}$ ternary complex, the 20-fold stronger interaction of Mn$_C^{2+}$ than Mg$_C^{2+}$ with the 2′-NH$_2$ group (see preceding section) provides an additional increase in the spec-

ificity of site C for Mn^{2+}, such that Mn$_C^{2+}$ binds 1000-fold stronger than Mg$_C^{2+}$, with a dissociation constant of ≤2 μM (Table 1).

The remarkably high affinity of metal site C suggests that M$_C$ interacts with multiple functional groups within the ribozyme active site, probably with one or more inner-sphere coordination to active site functional group(s). But what gives rise to the high specificity of this metal site for Mn^{2+} relative to Mg^{2+}? One possibility is that the ribozyme provides one or more nitrogen ligands, as nitrogen ligands interact with Mn^{2+} in preference to Mg^{2+}, whereas oxygen ligands do not typically provide a large advantage for interacting with Mn^{2+} [preceding section and Table 2, compounds **I**−**III** and **V**−**VI** for nitrogen ligands (K^{rel} = 12−630) versus compounds **IV** and **VII**−**XIII** for oxygen ligands (K^{rel} = 3.6−6.6)]. Alternatively or in addition, geometrical constraints within the binding site and the larger size of Mn^{2+} than Mg^{2+} may allow Mn$_C^{2+}$ to interact more favorably with multiple ligands within the ribozyme active site. The 100-fold higher affinity of 1,2-dihydroxybenzene dianion for Mn^{2+} relative to Mg^{2+} (Table 2, compound **XIV**) provides precedence for significantly stronger interaction of multiple oxygen ligands with Mn^{2+} than with Mg^{2+}. Identification of the functional groups on the ribozyme that provide ligands for M$_C$ (*30*) will be necessary for unraveling the molecular features that give rise to the high specificity of this metal site. Further, the high affinity and specificity of metal site C for Mn^{2+} introduce the possibility of future spectroscopic probing of the coordination environment and the dynamics of the metal site among the sea of metal ions bound to this ribozyme.

The approach described herein may provide a general tool for quantitatively probing the binding of specific functional metal ions to RNA and assessing the energetic effects of individual metal ion−RNA interactions. In general, divalent metal ions such as Mg^{2+} and Mn^{2+} can bind to the charged RNA backbone via polyelectrolyte effects; the majority of these metal ion sites involve outer-sphere coordination and have low affinity and specificity, with dissociation constants of >0.1 mM (e.g., *19, 52, 58-60,* and references cited therein). Nevertheless, strong binding of Mn^{2+} to RNA has been observed in several cases, and some metal sites also appear to have high specificity for Mn^{2+}. EPR investigation of Mn^{2+} binding to the hammerhead ribozyme suggested the presence of several metal sites with high Mn^{2+} affinity ($K_d^{Mn} ≤ 4 \mu$M; *52*). Folding of the hairpin ribozyme at its helical junction appears to involve two metal sites that bind Mn^{2+} at least 10-fold stronger than Mg^{2+}, with observed dissociation constants in the low micromolar range (*14* and references cited therein). Strong binding of multiple Mn^{2+} ions to tRNA ($K_d^{Mn} ≤ 10 \mu$M) has also been observed in equilibrium dialysis experiments (*59*), and proton NMR experiments indicated that one or more metal sites, located in the acceptor stem of tRNA, have at least 100-fold specificity for Mn^{2+} relative to Mg^{2+} (*61* and references cited therein). These observations indicate that the affinity and specificity of metal sites on RNA can be substantial. Nevertheless, to understand metal ion−RNA interactions, additional detailed structural studies will be required, in conjunction with more information about the affinity and specificity of metal ion sites in RNA and the energetics of their metal ion−ligand interactions.

Scheme 8
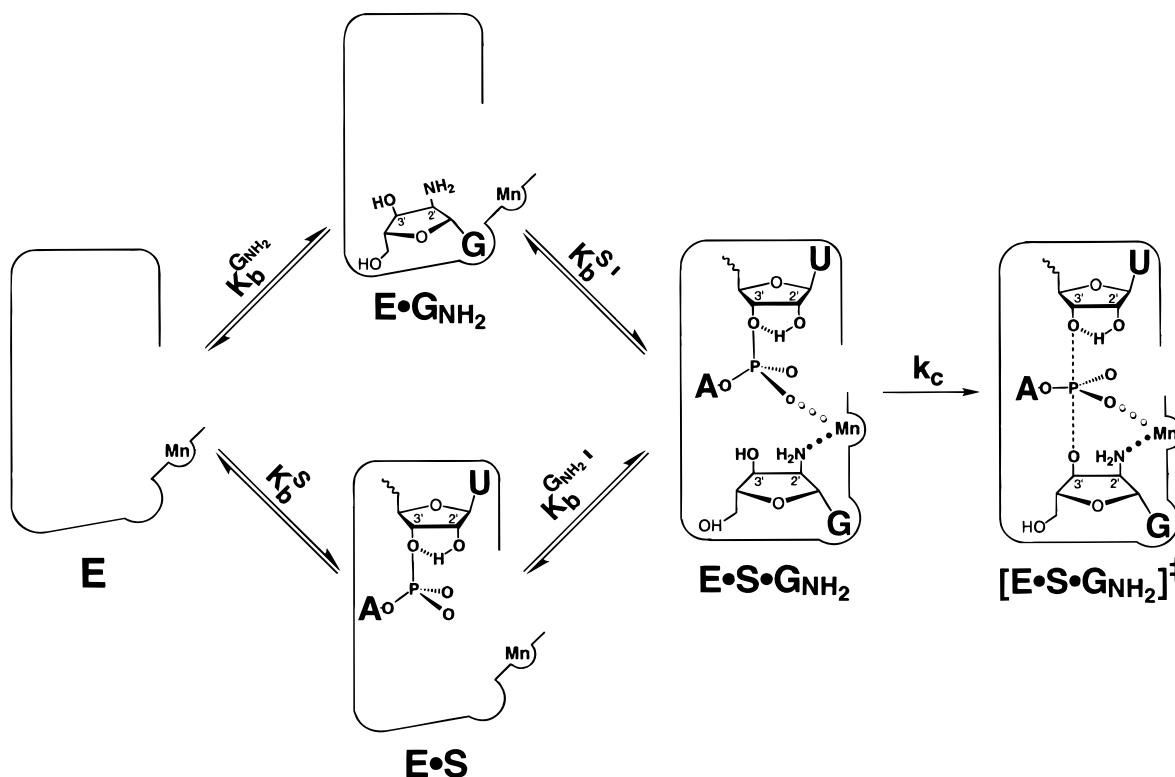
(C) Thermodynamic Fingerprint Allows Active Site Metal Ions To Be Distinguished. The affinities of metal ions for specific sites in the ribozyme and ribozyme·substrate complexes provide a fingerprint that allows these metal ions to be distinguished from one another. In this work, different fingerprints have allowed M_C to be distinguished from other metal ions and have facilitated the isolation of the effect of Mn^{2+} on individual reaction steps. The effect of Mn^{2+}_C on the binding of S was distinguished from the effect that stems from another Mn^{2+} ion that interacts with the A(+1) residue of S (Figure 6 and Results). Other Mn^{2+} ions also affect the reactivity of G and G_{NH_2} (see Figures 2 and 5), but the concentration dependences for these Mn^{2+} effects are distinct from that of Mn^{2+}_C, allowing the effect of these Mn^{2+} ions to be distinguished from the effect of Mn^{2+}_C. Recently, experiments analogous to those described herein have been used to determine the fingerprints of additional active site metal ions and have provided evidence for three distinct metal ions that interact with the 3′-atom of S and with the 3′- and 2′-moieties of G within the active site of the *Tetrahymena* ribozyme (Figure 1, M_A−M_C; Shan et al., submitted).

Role of M_C and the 2′-OH of G in Catalysis by the Tetrahymena Ribozyme. (A) Progression of the Interactions of Mn^{2+}_C along the Reaction Pathway. Replacing the 2′-OH of G with 2′-H reduces the rate of the chemical step more than 10^6-fold (*53, 54,* and unpublished results). This effect is consistent with an energetic penalty for desolvation of a Mg^{2+} ion and suggests that the 2′-OH of G plays a critical role in catalysis, probably via its associated metal ion. However, it is not obvious how this group and its associated metal ion contribute to catalysis, as the 2′-OH of G does not directly participate in the formation and breakage of covalent bonds. To learn about the interactions of M_C and

obtain clues to the catalytic role of this metal ion, the effect of Mn^{2+}_C on individual reaction steps was determined (Scheme 1). The results are discussed below in the context of the model in Scheme 8, which summarizes the interactions of Mn^{2+}_C along the reaction pathway.

Mn^{2+}_C binds strongly to E, but bound Mn^{2+}_C has at most a small effect on the binding of G_{NH_2} to E. This suggests that Mn^{2+}_C is not prealigned in the active site of the free ribozyme for interaction with the 2′-moiety of G or G_{NH_2}, and is depicted in Scheme 8 by having metal site C swung away from the active site in free E. Whether the Mn^{2+}_C·NH₂ interaction is made in the E·G_{NH_2} complex is determined by whether this interaction provides sufficient energy to drive the alignment of Mn^{2+}_C within the active site.[7] For simplicity, the E·G_{NH_2} complex is drawn lacking this interaction. Mn^{2+}_C also does not affect the binding of S to E, suggesting that there is no interaction between Mn^{2+}_C and S in the E·S complex. In contrast, Mn^{2+} gives a 20-fold increase in the binding of G_{NH_2} to the E·S complex, suggesting that Mn^{2+}_C is aligned and interacting with the 2′-moiety of G in the E·S·G_{NH_2} ternary complex. This direct metal ion interaction is depicted by the closed dots between Mn^{2+}_C and the 2′-nitrogen of G_{NH_2} in Scheme 8. Mn^{2+}_C also strengthens the binding of S to the E·G_{NH_2} complex by 20-fold, suggesting that Mn^{2+}_C also interacts with S in the ternary complex; this could be a direct or an indirect interaction (see below) and

---

[7] The observed 2-fold effect of Mn^{2+}_C on binding of G_{NH_2} to free E is consistent with this metal ion interaction being made a fraction of the time in the E·G_{NH_2} complex. This and additional unpublished observations suggest that the equilibrium constant for arranging this metal site with respect to the 2′-moiety of G and forming this interaction is close to 1.

is therefore depicted by open dots between Mn_C^{2+} and S in Scheme 8.

The results suggest that the interactions of Mn_C^{2+} drive a conformational change of the ribozyme that positions metal site C with respect to the 2′-moiety of G and with respect to the oligonucleotide substrate in the ternary complex. As described in the next section, this conformational change is presumably responsible for the coupled binding of S and G observed previously (*38, 62, 63*). Binding of Mn_C^{2+} does not affect the rate of reaction of the E·S·G_{NH_2} ternary complex, suggesting that the interactions made with the 2′-moiety of G and the substrate in the ternary complex are maintained in the transition state (Scheme 8, [E·S·G_{NH_2}]‡). Possible roles of M_C in catalysis are then discussed in the following sections.

(B) An Integral Role of M_C in the Coupling between S and G. There is coupling between the oligonucleotide substrate and the guanosine nucleophile; i.e., S and G strengthen the binding of one another (*38, 63*; see also Scheme 1: K_d^S vs $K_d^{S\prime}$ and $K_{b,Mg}^{G_X}$ vs $K_{b,Mg}^{G_X}{}\prime$ (red numbers for G)]. This coupling suggests that the binding of S or G drives a change of the ribozyme into a conformation in which S and G are better aligned with respect to groups within the active site. However, when the 2′-OH of G is replaced by -NH_2, the coupling between the oligonucleotide substrate and the nucleophile is lost with metal site C occupied by a Mg^{2+} [Scheme 1: $K_{d,Mg}^S \approx K_{d,Mg}^S{}\prime$ (blue number for G_{NH_2}) and $K_{b,Mg}^{G_{NH_2}} \approx K_{b,Mg}^{G_{NH_2}}{}\prime$]. This loss of coupling presumably arises from the weaker interaction of Mg^{2+} with the 2′-NH_2 group relative to 2′-OH (Scheme 7A,C). The stronger interaction of Mn^{2+} than Mg^{2+} with the amino group (Scheme 7C,D, Table 2) would then allow coupling to be restored, as was indeed observed upon replacement of Mg_C^{2+} by Mn^{2+} [Scheme 1: $K_{d,Mn}^S$ vs $K_{d,Mn}^S{}\prime$ (blue number for G_{NH_2}) and $K_{b,Mn}^{G_{NH_2}}$ vs $K_{b,Mn}^{G_{NH_2}}{}\prime$]. Thus, M_C is intimately involved in the coupling between the oligonucleotide substrate and the guanosine nucleophile.

A role of M_C in the coupling between S and G is further supported by the observation that the interaction of Mn_C^{2+} with G_{NH_2} and the oligonucleotide requires the reactive phosphoryl group, as the reactive phosphoryl group was also shown to be required for the coupled binding between oligonucleotides and guanosine (*38*). In addition, previous work showed that below 10 °C, the guanosine nucleophile can bind as strongly to E as to the E·S complex, suggesting that the ribozyme exists in a conformation with active site groups already aligned to interact with S and G in the binary complexes at low temperature, as in the E·S·G ternary complex at higher temperature (*62*). Similarly, Mn_C^{2+} increases the binding of G_{NH_2} to free E at 0 °C, suggesting that the interaction of Mn_C^{2+} with G_{NH_2} can be made even in the absence of bound S at low temperature (unpublished results). These parallels between the interactions of Mn_C^{2+} and the coupling of G with S provide strong support for an integral role of M_C in the coupling between the oligonucleotide substrate and the guanosine nucleophile.

How does M_C communicate with the reactive phosphoryl group? The simplest model would be a direct coordination of M_C to one of the nonbridging oxygens of the reactive phosphoryl group. However, thio-substitution at each of these

Scheme 9
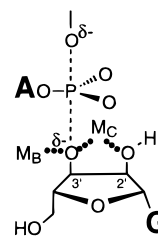
oxygens does not affect the binding of Mn_C^{2+} or the energetics of the Mn_C^{2+}·G_{NH_2} interaction, providing no indication of a direct interaction (unpublished results). Alternatively, the communication between M_C and the reactive phosphoryl group could be mediated by a network of active site interactions. Identification of functional groups on the ribozyme that provide additional ligands for M_C may help elucidate such a network and could be important for further probing the communication between M_C and the reactive phosphoryl group. Spectroscopic methods that distinguish between inner- and outer-sphere coordination may also help elucidate the nature of the communication between M_C and the reactive phosphoryl group.

(C) Role of M_C and the 2′-OH of G in Catalysis. Recent studies suggest that two distinct metal ions interact with the 3′- and 2′-moieties of G, referred to as M_B and M_C, respectively (Figure 1; Shan et al., submitted). An appealing model is that M_C also interacts with the 3′-OH of G (*22*), acting in concert with M_B to deprotonate the 3′-OH at physiological pH and activate it for nucleophilic attack (Scheme 9; *25*). Activation of a nucleophile by interaction with two metal ions has been proposed for a different RNA enzyme based on molecular dynamics simulation (*64*) and for several protein enzymes (e.g., *65−67*). This mechanistic model remains to be tested.

Alternatively or in addition, M_C may play a role in the positioning of the guanosine nucleophile and the organization of the ribozyme active site (see also *68−70* and references cited therein). As described above, in addition to a direct coordination to the 2′-nitrogen of G_{NH_2}, Mn_C^{2+} also interacts, directly or indirectly, with the reactive phosphoryl group; these interactions drive a conformational change on the ribozyme that allows coupling between S and G. These results strongly suggest that M_C may be used to align the guanosine nucleophile with respect to the reactive phosphoryl group and possibly with respect to other catalytic groups within the active site, thereby facilitating the reaction.

But does a contribution of M_C to active site alignment remain at low temperature, where the ribozyme appears to no longer require the energy from interactions of Mn_C^{2+} with G_{NH_2} and S to drive the transition to an aligned conformation (Scheme 8)? The effect of replacing the 2′-OH group of G by 2′-H remains more than 10^6-fold at 0 °C (unpublished results), suggesting that M_C is still crucial for catalysis at low temperature. Although it is possible that M_C plays no role in alignment beyond its involvement in coupling at the higher temperatures, a larger or additional roles of M_C would not have been exposed. This is because replacing the 2′-OH of G with -NH_2 and the Mg^{2+} at site C with Mn^{2+} modulates the strength of the interaction of M_C with the 2′-moiety of G but do not remove this metal ion or disrupt its

Scheme 10
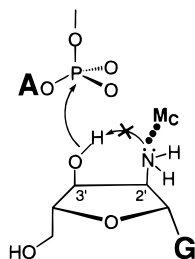
interactions with other groups. Indeed, the remarkably high affinity of site C for Mn^{2+} suggests that M_C is situated within a network of interactions in the ribozyme core; this network may be critical for alignment of other active site metal ions and functional groups required for efficient catalysis.

Finally, the results herein allow evaluation of catalytic models in which the 2′-OH of G acts as a general base or proton shuttle to help deprotonate the 3′-hydroxyl group. The 2′-NH_2 group of G_{NH_2} contains only a single lone pair of electrons, and this lone pair interacts with M_C, leaving no electron pair to accept a proton from the 3′-OH (Scheme 10). Nevertheless, the reactivity of G_{NH_2} is within 5-fold of G, strongly suggesting that the 2′-functional group of G does not act as a general base or proton shuttle.

General Implications. The approach described herein, use of metal ion specificity switch combined with quantitative analysis to obtain thermodynamic fingerprints for individual metal ions, may provide a general approach for studying the role of metal ions in RNA function. Thermodynamic fingerprints provide a powerful tool for identifying and distinguishing distinct metal ions. The ability to distinguish between active site metal ions then facilitates the isolation of the energetic effect of individual metal ion interactions, providing clues to the mechanism of action for each metal ion and facilitating tests of mechanistic proposals. Thermodynamic fingerprints also provide a readout of the energetic consequences of metal ion−RNA interactions, allowing the structural and energetic properties of individual metal sites within folded RNA to be probed. Finally, the fingerprints obtained for M_C and other active site metal ions (Shan et al., submitted) will facilitate the identification and study of functional groups on the ribozyme that provide additional ligands for each metal ion.

ACKNOWLEDGMENT

REFERENCES

1. Fersht, A. (1984) in *Enzyme Structure and Mechanism*, p 161, W. H. Freeman and Company, New York.
2. Crothers, D. M. (1979) in *Transfer RNA: Structure, Properties, and Recognition*, pp 163−176, Cold Spring Harbor Laboratory Press, Plainview, NY.
3. Quigley, G. J., Teeter, M. M., and Rich, A. (1978) *Proc. Natl. Acad. Sci. U.S.A. 75*, 64−68.
4. Saenger, W. (1984) in *Principles of Nucleic Acid Structure*, pp 201−209, 343−346, Springer-Verlag, New York.
5. Bujalowski, W., Graester, E., McLaughlin, L. W., and Porschke, D. (1986) *Biochemistry 25*, 6365−6371.
6. Celander, D. W., and Cech, T. R. (1991) *Science 251*, 401−407.
7. Pan, T., Long, D. M., and Uhlenbeck, O. C. (1993) in *The RNA World*, pp 271−302, Cold Spring Harbor Laboratory Press, Cold Spring Harbor, NY.
8. Pan, T. (1995) *Biochemistry 34*, 902−909.
9. Beebe, J. A., Kurz, J. C., and Fierke, C. A. (1996) *Biochemistry 35*, 10493−10505.
10. Bassi, G. S., Murchie, A. I. H., and Lilley, D. M. J. (1996) *RNA 2*, 756−768.
11. Cate, J. H., and Doudna, J. A. (1996) *Structure 4*, 1221−1229.
12. Cate, J. H., Gooding, A. R., Podell, E., Zhou, K., Golden, B. L., Kundrot, C. E., Cech, T. R., and Doudna, J. A. (1996) *Science 273*, 1678−1685.
13. Cate, J. H., Hanna, R. L., and Doudna, J. A. (1997) *Nat. Struct. Biol. 7*, 553−558.
14. Walter, F., Murchie, A. I. H., Thomson, J. B., and Lilley, D. M. J. (1998) *Biochemistry 37*, 14195−14203.
15. Draper, D. E. (1996) *Trends Biochem. Sci. 21*, 145−149.
16. Draper, D. E. (1996) *Nat. Struct. Biol. 3*, 397−400.
17. Correll, C. C., Freeborn, B., Moore, P. B., and Steitz, T. A. (1997) *Cell 91*, 705−712.
18. Wu, M., and Tinoco, I., Jr. (1998) *Proc. Natl. Acad. Sci. U.S.A. 95*, 11555−11560.
19. Gluick, T. C., Wills, N. M., Gesteland, R. F., and Draper, D. E. (1997) *Biochemistry 36*, 16173−16186.
20. Piccirilli, J. A., Vyle, J. S., Caruthers, M. H., and Cech, T. R. (1993) *Nature 361*, 85−88.
21. Scott, E. C., and Uhlenbeck, O. C. (1999) *Nucleic Acids Res. 27*, 479−484.
22. Sjögren, A.-S., Pettersson, E., Sjöberg, B.-M., and Strömberg, R. (1997) *Nucleic Acids Res. 25*, 648−653.
23. Sontheimer, E. J., Sun, S., and Piccirilli, J. (1997) *Nature 388*, 801−805.
24. Warnecke, J. M., Furste, J. P., Hardt, W.-D., Erdmann, V. A., and Hartmann, R. K. (1996) *Proc. Natl. Acad. Sci. U.S.A. 93*, 8924−8928.
25. Weinstein, L. B., Jones, B. C., Cosstick, R., and Cech, T. R. (1997) *Nature 388*, 805−808.
26. Chen, Y., Li, X., and Gegenheimer, P. (1997) *Biochemistry 36*, 2425−2438.
27. Burgers, P. M. J., and Eckstein, F. (1979) *J. Biol. Chem. 254*, 6889−6893.
28. Burgers, P. M. J., and Eckstein, F. (1980) *J. Biol. Chem. 255*, 8229−8233.
29. Connolly, B. A., and Eckstein, F. (1981) *J. Biol. Chem. 256*, 9450−9456.
30. Christian, E. L., and Yarus, M. (1993) *Biochemistry 32*, 4475−4480.
31. Jaffe, E. K., and Cohn, M. (1978) *J. Biol. Chem. 253*, 4823−4825.
32. Peracchi, A., Beigelman, L., Scott, E. C., Uhlenbeck, O. C., and Herschlag, D. H. (1997) *J. Biol. Chem. 272*, 26822−26826.
33. Herschlag, D., and Cech, T. R. (1990) *Biochemistry 29*, 10159−10171.
34. Herschlag, D., and Cech, T. R. (1990) *Biochemistry 29*, 10172−10180.
35. Cech, T. R., and Herschlag, D. (1996) in *Nucleic Acids and Molecular Biology,* pp 1−17, Springer, Berlin.
36. Zaug, A. J., Grosshans, C. A., and Cech, T. R. (1988) *Biochemistry 27*, 8924−8931.
37. Herschlag, D., Eckstein, F., and Cech, T. R. (1993) *Biochemistry 32*, 8299−8311.
38. McConnell, T. S., Cech, T. R., and Herschlag, D. H. (1993) *Proc. Natl. Acad. Sci. U.S.A. 90*, 8362−8366.
39. Shan, S., Narlikar, G. J., and Herschlag, D. (1999) *Biochemistry 38*, 10976−10988.
40. Herschlag, D., Eckstein, F., and Cech, T. R. (1993) *Biochemistry 32*, 8312−8321.
41. Herschlag, D., Piccirilli, J. A., and Cech, T. R. (1991) *Biochemistry 30*, 4844−4854.

42. Strobel, S. A., and Cech, T. R. (1996) *Biochemistry 35*, 1201−1211.
43. Knitt, D. S., Narlikar, G. J., and Herschlag, D. (1994) *Biochemistry 33*, 13864−13879.
44. McConnell, T. S. (1995) Ph.D. Thesis, University of Colorado, Boulder, CO.
45. Narlikar, G. J., Khosla, M., Usman, N., and Herschlag, D. (1997) *Biochemistry 36*, 2465−2477.
46. Rose, I. A., O'Connell, E. L., Litwin, S., and Bar Tana, J. (1974) *J. Biol. Chem. 249*, 5163−5168.
47. McConnell, T. S., Herschlag, D. H., and Cech, T. R. (1997) *Biochemistry 36*, 8293−8303.
48. Goody, R. S., Frech, M., and Wittinghofer, A. (1991) *Trends Biochem. Sci. 16*, 327−328.
49. Herschlag, D., and Khosla, M. (1994) *Biochemistry 33*, 5291−5297.
50. Latham, J. A., and Cech, T. R. (1989) *Science 245*, 276−282.
51. Wang, J. F., and Cech, T. R (1994) *J. Am. Chem. Soc. 116*, 4178−4182.
52. Horton, T. E., Clardy, D. R., and DeRose, V. J. (1998) *Biochemistry 37*, 18094−18101.
53. Bass, B. L., and Cech, T. R. (1986) *Biochemistry 25*, 4473−4477.
54. Tanner, N. K., and Cech, T. R. (1987) *Biochemistry 26*, 3330−3340.
55. Martell, A. E., and Smith, R. M. (1976) in *Critical Stability Constants,* Plenum, New York.
56. Sille'n, L. G., and Martell, A. E. (1964) in *Stability Constants of Metal−Ligand Complexes, Special publication 17,* The Chemical Society, London.
57. Pearson, R. G. (1966) *Science 151*, 172−177.
58. Anderson, C. F., and Record, M. T. (1995) *Annu. Rev. Phys. Chem. 46*, 657−700.
59. Schreier, A. A., and Schimmel, P. R. (1974) *J. Mol. Biol. 86*, 601−620.
60. Yamada, A., Akasaka, K., and Hatano, H. (1976) *Biopolymers 15*, 1315−1331.
61. Ott, G., Arnold, L., and Limmer, S. (1993) *Nucleic Acids Res. 21*, 5859−5864.
62. McConnell, T. S., and Cech, T. R. (1995) *Biochemistry 34*, 4056−4067.
63. Bevilacqua, P. C., Li, Y., and Turner, D. H. (1994) *Biochemistry 33*, 11340−11348.
64. Hermann, T., Auffinger, P., Scott, W. G., and Westhof, E. (1997) *Nucleic Acids Res. 25*, 3421−3427.
65. Fabiane, S. M., Sohi, M. K., Wan, T., Payne, D. J., Bateson, J. H., Mitchell, T., and Sutton, B. (1998) *Biochemistry 37*, 12404−12411.
66. Heikinheimo, P., Lehtonen, J., Baykov, A., Lahti, R., Cooperman, B. S., and Goldman, A. (1996) *Structure 15*, 1491−1508.
67. Kanyo, Z. F., Scolnick, L. R., Ash, D. E., and Christianson, D. W. (1996) *Nature 383*, 554−557.
68. Turner, D. H., Li, Y., Fountain, M., Profenno, L., and Bevilacqua, P. C. (1996) *Nucleic Acids Mol. Biol. 10*, 19−32.
69. Li, Y., and Turner, D. H. (1997) *Biochemistry 36*, 11131−11139.
70. Profenno, L. A., Kierzek, R., Testa, S. M., and Turner, D. H. (1997) *Biochemistry 36*, 12477−12485.